# Hydrodynamics of pulsed jetting in juvenile and adult brief squid *Lolliguncula brevis*: evidence of multiple jet 'modes' and their implications for propulsive efficiency

Ian K. Bartol[1],*, Paul S. Krueger[2], William J. Stewart[1] and Joseph T. Thompson[3]

[1]Department of Biological Sciences, Old Dominion University, Norfolk, VA 23529, USA, [2]Department of Mechanical Engineering, Southern Methodist University, Dallas, TX 75275, USA and [3]Department of Biology, Franklin and Marshall College, Lancaster, PA 17604, USA

*Author for correspondence (e-mail: ibartol@odu.edu)

## SUMMARY

The dynamics of pulsed jetting in squids throughout ontogeny is not well understood, especially with regard to the development of vortex rings, which are common features of mechanically generated jet pulses (also known as starting jets). Studies of mechanically generated starting jets have revealed a limiting principle for vortex ring formation characterized in terms of a 'formation number' (*F*), which delineates the transition between the formation of isolated vortex rings and vortex rings that have 'pinched off' from the generating jet. Near *F*, there exists an optimum in pulse-averaged thrust with (potentially) low energetic cost, raising the question: do squids produce vortex rings and if so, do they fall near *F*, where propulsive benefits presumably occur? To better understand vortex ring dynamics and propulsive jet efficiency throughout ontogeny, brief squid *Lolliguncula brevis* ranging from 3.3 to 9.1 cm dorsal mantle length (*DML*) and swimming at speeds of 2.43–22.2 cm s$^{-1}$ (0.54–3.50 *DML* s$^{-1}$) were studied using digital particle image velocimetry (DPIV). A range of jet structures were observed but most structures could be classified as variations of two principal jet modes: (1) jet mode I, where the ejected fluid rolled up into an isolated vortex ring; and (2) jet mode II, where the ejected fluid developed into a leading vortex ring that separated or 'pinched off' from a long trailing jet. The ratio of jet length [based on the vorticity extent (*L*$_\omega$)] to jet diameter [based on peak vorticity locations (*D*$_\omega$)] was <3.0 for jet mode I and >3.0 for jet mode II, placing the transition between modes in rough agreement with *F* determined in mechanical jet studies. Jet mode II produced greater time-averaged thrust and lift forces and was the jet mode most heavily used whereas jet mode I had higher propulsive efficiency, lower slip, shorter jet periods and a higher frequency of fin activity associated with it. No relationship between *L*$_\omega$/*D*$_\omega$ and speed was detected and there was no apparent speed preference for the jet modes within the speed range considered in this study; however, propulsive efficiency did increase with speed partly because of a reduction in slip and jet angle with speed. Trends in higher slip, lower propulsive efficiency and higher relative lift production were observed for squid <5.0 cm *DML* compared with squid ≥5.0 cm *DML*. While these trends were observed when jet mode I and II were equally represented among the size classes, there was also greater relative dependence on jet mode I than jet mode II for squid <5.0 cm *DML* when all of the available jet sequences were examined. Collectively, these results indicate that ~5.0 cm *DML* is an important ontogenetic transition for the hydrodynamics of pulsed jetting in squids. The significance of our findings is that from early juvenile through to adult life stages, *L. brevis* is capable of producing a diversity of vortex ring-based jet structures, ranging from efficient short pulses to high-force longer duration pulses. Given that some of these structures had *L*$_\omega$/*D*$_\omega$s near *F*, and *F* represented the delineation between the two primary jet modes observed, fluid dynamics probably played an integral role in the evolution of squid locomotive systems. When this flexibility in jet dynamics is coupled with the highly versatile fins, which are capable of producing multiple hydrodynamic modes as well, it is clear that squid have a locomotive repertoire far more complex than originally thought.

Key words: hydrodynamics, ontogeny, squid, swimming, vortex rings.

## INTRODUCTION

Aquatic locomotors propel themselves by transferring momentum into the water *via* regulated bursts of vorticity, with the three-dimensional topology of the wake depending heavily on locomotive style and Reynolds number (*Re*). As swimmers undergo critical morphological, ecological and behavioral changes throughout ontogeny, they employ different swimming styles, each with a potentially different propulsive efficiency. The interspecific swimming strategies and hydrodynamics of a variety of swimmers spanning many orders of magnitude have been summarized broadly elsewhere (see Daniel et al., 1992; Lighthill, 1975; Wu, 1977), and the most thorough treatment of intraspecific scaling effects on swimming kinematics and hydrodynamics have been performed on fishes (e.g. Batty, 1984; Fuiman and Batty, 1997; Fuiman and Webb,

1988; Hunter, 1972; McHenry and Lauder, 2005; Müller et al., 2000). In general, inertial force generation (e.g. lift-based thrust and acceleration reaction) becomes increasingly more important as fishes grow larger and faster, with viscous force generation (e.g. drag-based thrust) playing more prominent roles at low/intermediate *Re* (Videler, 1993; Fuiman and Batty, 1997; McHenry et al., 2003; Müller et al., 2000; Webb and Weihs, 1986). Because body undulations in fishes (and other animals) can generate both inertial and viscous propulsive forces, undulatory mechanisms are particularly effective at generating thrust over a wide range of flow regimes throughout ontogeny (McHenry et al., 2003; Videler, 1993).

The scaling of swimming dynamics is less well understood in aquatic invertebrates compared with fishes, although the

hydrodynamics of swimming throughout ontogeny has been examined in brine shrimp (Williams, 1994), spiny lobster (Nauen and Shadwick, 1999), scallops (Cheng and DeMont, 1996; Dadswell and Weihs, 1990), jellyfish (McHenry and Jed, 2003) and squid (Bartol et al., 2001b; Thompson and Kier, 2002). In contrast to fishes, squids and many jellyfishes do not rely on undulatory mechanisms over their entire range of life history stages. Jellyfish, such as *Aurelia aurita,* are capable of generating thrust by both paddle and jet mechanisms but rely primarily on jetting throughout ontogeny with only negligible thrust generation by paddling of the bell margin (McHenry and Jed, 2003), although some jellyfish lineages do rely heavily on rowing propulsion throughout development (see Costello et al., 2008). Hatchling squid, i.e. paralarvae, rely predominantly on a pulsatile jet at intermediate *Re*, and their rudimentary fins, which are capable of producing undulatory/oscillatory forces at other life history stages, play only a minor role in propulsion (Bartol et al., 2008; Bartol et al., 2009; Boletzky, 1987; Hoar et al., 1994; O'Dor et al., 1986). At juvenile and adult life stages, squid rely more heavily on undulatory/ oscillatory fin activity during low and intermediate speed propulsion to complement their pulsed jet (Anderson and DeMont, 2005; Bartol et al., 2001a; Bartol et al., 2001b; Hoar et al., 1994; O'Dor, 1988). Although the balance of propulsion is tipped more towards fin activity than jet propulsion in some mesopelagic and bathypelagic adult squid (Vecchione et al., 2001; Vecchione et al., 2002), the pulsed jet remains the foundation of the propulsive system in most squids throughout ontogeny.

Despite playing a prominent role in the propulsion of squids, little is known about the hydrodynamics of the pulsed jet of squids throughout ontogeny. Based on kinematic measurements, Bartol et al. (Bartol et al., 2001b) made lift and thrust predictions of the fins and jet for brief squid *Lolliguncula brevis* from 1.8 to 8.9 cm dorsal mantle length (*DML*) and estimated jet propulsive efficiency from flow visualizations. Thompson and Kier (Thompson and Kier, 2001; Thompson and Kier, 2002) examined the mechanics of the mantle in *Sepioteuthis lessoniana* (0.5–4.0 cm *DML*) using kinematic and force transducer measurements. However, neither study involved direct quantification of the structure of the jet throughout ontogeny.

Vortex rings presumably play an important role in jet hydrodynamics of squid as they move through different life history stages. Vortex rings, which develop as the vortex sheet in the jet boundary layer rolls up and separates at the funnel aperture, are critical coherent structures for momentum transfer, providing important thrust benefits *via* acceleration of ambient fluid through entrainment and added mass effects (Krueger and Gharib, 2003; Krueger and Gharib, 2005). Although vortex rings are prominent structures in mechanically generated jets, occurring both in an isolated form during short jets and as a leading component of a vortex ring/trailing jet complex during long jets (Gharib et al., 1998; Rosenfeld et al., 1998; Mohseni et al., 2001; Krueger et al., 2003; Krueger et al., 2006), their presence in the wakes of jetting squid is less clear, especially with regard to scaling. In adult long-finned squid *Doryteuthis pealeii* [formerly *Loligo pealeii* (see Vecchione et al., 2005) *DML*=27.1±3.0 cm (means ± s.d.)], Anderson and Grosenbaugh did not observe consistent vortex rings, either in their individual form or as discernible leading structures in highly elongated jets (Anderson and Grosenbaugh, 2005). In contrast, early life history stages of *D. pealeii*, i.e. paralarvae (~0.18 cm *DML*), produce spherical and elongated vortex rings with lower aspect ratios than the long emissions of fluid observed in adults (Bartol et al., 2009), suggesting that vortex ring structure changes significantly with life history stage in *D. pealeii*. Based on dye injection

experiments, there is qualitative evidence that juvenile *L. brevis* (~4.2 cm *DML*) also produce vortex rings during jetting like *D. pealeii* paralarvae (see Bartol et al., 2001b) but the structures were not quantified using digital particle image velocimetry (DPIV) or other global flow characterization techniques. Consequently, significant gaps in our understanding of vortex ring development throughout ontogeny in squids remain.

Previous investigations of mechanically generated jets have demonstrated a limiting principle for vortex ring formation characterized in terms of a dimensionless formation number (Gharib et al., 1998). This formation number (*F*) occurs when the ratio of length of the ejected plug of fluid (*L*) to the diameter of the jet aperture (*D*) is ~4 for jets issuing into quiescent fluid. For jet pulses where *L*/*D*>*F*, the vortex ring stops entraining circulation, impulse and energy from the generating jet and separates from the jet. Different jet structures, therefore, form depending on the length of the jet, with vortex rings or puffs developing during short jets (*L*/*D*≤4) and vortex rings pinched off from the generating jet during long jets (*L*/*D*>4) (Gharib et al., 1998; Rosenfeld et al., 1998; Mohseni et al., 2001; Krueger et al., 2003; Krueger et al., 2006). As *L*/*D* approaches *F*, an optimum in per-pulse-averaged thrust is realized (Krueger and Gharib, 2003). Currently, it is not known whether juvenile and adult squid ~1–20 cm *DML* produce jets near *F*, where propulsive efficiency gains may occur, or produce multiple wake modes, possibly with and without vortex rings. Moreover, it is not clear whether wake structure and propulsive jet efficiency change appreciably with life history stage in squid or even if vortex rings are more efficient than ring/jet complexes.

In this paper, jet dynamics over a size range of juvenile and adult brief squid *L. brevis* (~3–9 cm *DML*) were studied using DPIV. The primary objectives of this study were to determine (1) whether consistent vortex ring formation occurs and, if so, whether or not it leads to gains in propulsive efficiency, (2) whether distinct jet structures or 'modes' are present, and (3) whether jet properties and propulsive efficiency change along a continuum of life history stages from juveniles to adults. The DPIV technique allows for the direct measurement of bulk properties of the jet wake (e.g. circulation, impulse, kinetic energy) and other jet features (e.g. jet length, jet diameter, jet velocity, vorticity structure). These jet properties were used both to characterize wake structure and to calculate propulsive efficiency. Some of the questions above were addressed briefly in a previously published overview paper on squid jetting throughout ontogeny (see Bartol et al., 2008) but we present a more detailed and expansive data set in this paper.

## MATERIALS AND METHODS
### Animals and maintenance

Juvenile and adult *Lolliguncula brevis* Blainville used in this project were either shipped from the National Resource Center for Cephalopods (NRCC) or captured by otter trawl in Wachapreague, VA, USA. All squid were kept in 1.2 m diameter circular tanks with re-circulating seawater using protocols detailed in Hanlon et al. (Hanlon et al., 1983) and Hanlon (Hanlon, 1990). In all >300 squid, ranging in size from 1.1 to 9.1 cm *DML*, were collected/shipped for this experiment. A large number of these squid were <3 cm *DML* but unfortunately squid 1–3 cm *DML* were not cooperative during experiments and thus no useable DPIV data were obtained for this size range. Useable DPIV data on 40 *L. brevis*, ranging from 3.3 to 9.1 cm *DML* and swimming at speeds of 2.43–22.2 cm s$^{-1}$ (0.54–3.50 *DML* s$^{-1}$), were collected. Vorticity and velocity fields were measured for 248 recorded jet sequences, which allowed for the determination of general jet features, and 59 of these jet

sequences were deemed acceptable for more detailed analysis using criteria defined in the subsection 'Data processing and analysis'.

### DPIV experiments

The DPIV procedure used in this experiment was similar to that used in previous studies (Bartol et al., 2008; Bartol et al., 2009) but a brief description is repeated here for convenience. The DPIV experiments were conducted in a water tunnel with a $15 \times 15 \times 44$ cm working section [Model 502(S), Engineering Laboratory Design, Lake City, MN, USA] filled with aerated, artificial seawater (24°C, 30 PSU) seeded with near neutrally buoyant, silver-coated, hollow glass spheres (mean diameter=14 μm, Potters Industries, Valley Forge, PA, USA). Each squid was placed in the water tunnel and trained to swim against a $3–6$ cm s$^{-1}$ current for 15–45 min, after which speed was increased in a stepwise manner until the squid could no longer keep pace with free-stream flow. During each speed interval, DPIV and kinematic data were collected. The data collection procedure involved illuminating the seeded particles in a parasagittal plane using two (A and B) pulsed Nd:YAG lasers and a laser optical arm (wavelength=532 nm, power rating 350 mJ pulse$^{-1}$; LaBest Optronics, Beijing, China). Each laser was operated at 15 Hz (7 ns pulse duration) with a 1–4 ms separation between laser A and B pulses. Three video cameras, each connected to a separate CL-160 capture card (IO Industries, London, ON, Canada), were used: (1) a UNIQ UP-1830 'double-shot' video camera [UNIQ Vision, Santa Clara, CA, USA; $1024 \times 1024$ pixel resolution; paired images collected at 15 Hz; $8 \times 8 – 12 \times 12$ cm field of view (FOV)] positioned laterally to the working section to record particle movements; (2) a DALSA 1M150 video camera (DALSA Corp., Waterloo, ON, Canada; $1024 \times 1024$ pixel resolution, frame rates of 15–100 Hz, $12 \times 12$ cm FOV) positioned laterally to record fin, mantle and funnel movements; and (3) a second DALSA 1M150 video camera ($1024 \times 1024$ pixel resolution, frame rates of 15–100 Hz, $8 \times 8 – 12 \times 12$ cm FOV) positioned underneath the working section to record fin, mantle and funnel movements.

The lasers and DPIV camera were triggered and synchronized using a timing program developed by Dr Morteza Gharib's Lab (California Institute of Technology, Pasadena, CA, USA), a PCI-6602 counter/timing card (National Instruments, Austin, TX, USA) and a BNC-565 pulse generator (Berkeley Nucleonics, San Rafael, CA, USA). A 4003A signal generator (B&K Precision, Yorba Linda, CA, USA) was used to trigger the DALSA cameras at 15–100 Hz, with 50 Hz being the most frequently used trigger rate. All three cameras and the laser guide arm were mounted to a motorized 4-axis traverse system (Techno-Isel, New Hyde Park, NY, USA), which allowed us to move the laser sheet and cameras to the regions of the tunnel where the squid was located. The laser sheet was projected vertically from underneath the working section with a streamwise orientation. Using the traverse system, the laser arm was positioned so that the long axis of the squid funnel was within the projected laser plane.

Separate lighting and spectral filters were used with each camera. A series of four 40 W lights outfitted with a color gel #27 filter (transmits wavelengths >600 nm) provided illumination for the high-speed DALSA cameras, while the laser light (532 nm) provided the illumination for the DPIV UNIQ camera. A Kodak Wratten 32 magenta filter (blocks wavelengths 520–600 nm) was mounted to the lens of the laterally-oriented DALSA camera to prevent overexposure of laser light, and an IR filter and a Kodak Wratten 58 green filter (transmits wavelengths of 410–600 nm) were mounted to the UNIQ UP-1830CL camera lens to prevent overexposure from the 40 W halogen lights. A filter was not used with the DALSA camera positioned underneath the working section so that the laser sheet was visible in images.

### Data processing and analysis

For analysis of the DPIV data, each image was subdivided into a matrix of $32^2$ pixel interrogation windows. Using a 16 pixel offset (50% overlap), cross-correlation was used to determine the particle displacements within interrogation windows on the paired images using *PixelFlow*™ software (FG Group LLC, San Marino, CA USA), following an algorithm similar to that used by Willert and Gharib (Willert and Gharib 1991). Outliers, defined as particle shifts that were three pixels greater than their neighbors, were removed and the data were subsequently smoothed to remove high frequency fluctuations. Window shifting was performed followed by a second iteration of outlier removal and smoothing (Westerwheel et al., 1997). Using *PixelFlow*™ software, velocity vector and vorticity contour fields were determined for all experimental trials.

A smaller subset of the data was selected for further detailed kinematic, propulsive efficiency and jet property analyses, using several criteria: (1) the jet sequence needed to be representative of the target speed range and size class, which was determined from velocity and vector fields; (2) the jet flows had to be completely bisected by the laser, which was confirmed from lateral views (the funnel needed to be illuminated evenly by the laser sheet) and underneath views (the sheet needed to be positioned nearly coincident with the longitudinal axis of the funnel); and (3) the squid needed to be swimming steadily against the current during the target jet sequence and the sequences immediately preceding and following the target sequence. Given that two principal jet modes emerged (see Results), an effort was made to include representative sequences of both jet modes for five different size classes of *L. brevis*. The size classes and speed ranges considered were as follows: (1) 3.0–3.9 cm *DML*, in which six squid swimming over speeds of 1.01–3.49 *DML* s$^{-1}$ during nine jet sequences were considered; (2) 4.0–4.9 cm *DML*, in which eight squid swimming over speeds of 1.06–2.27 *DML* s$^{-1}$ during 16 jet sequences were considered; (3) 5.0–5.9 *DML*, in which seven squid swimming over speeds of 0.99–2.61 *DML* s$^{-1}$ during 14 jet sequences were considered; (4) 6.0–6.9 cm *DML*, in which five squid swimming over speeds of 0.90–3.00 *DML* s$^{-1}$ during 10 jet sequences were considered; and (5) ≥7.0 cm *DML*, in which five squid swimming over speeds of 1.04–2.17 *DML* s$^{-1}$ during 10 jet sequences were considered.

For these selected sequences, mantle diameter, funnel diameter ($D_F$), mantle contraction period, mantle refilling period, body position and fin motion were measured from the high-speed DALSA footage using the National Institute of Health's public domain program ImageJ (http://rsbweb.nih.gov/ij/) and Matlab code written by T. Hedrick (University of North Carolina, Chapel Hill, NC, USA, available at http://www.unc.edu/~thedrick/software1.html).

For analysis of jet flows, the region of the flow containing the jet was identified based on the vorticity field and the following operations were performed for each frame in the selected jet sequence. The following procedures were previously described (Bartol et al., 2009) but are included here for convenience: (1) the location of the jet centerline and the components of the unit vectors in the longitudinal ($\hat{n}_z$) and radial ($\hat{n}_r$) directions relative to the jet centerline (see Fig. 4) were computed using one of two user-selected methods. (a) For method 1, the jet centerline was centered on the centroid of the jet region over which the jet velocity magnitude was above a specified threshold (generally ~20% of peak jet velocity). The orientation (slope) of the jet centerline was determined from the weighted average of the jet velocity vector orientation in the

same region used to identify the jet centroid. This method worked well for longer jets. (b) For method 2, the jet centerline was centered between the locations of the positive and negative peak vorticity and was oriented perpendicular to the line connecting the vorticity peaks. The locations of the vorticity peaks were determined from the centroids of vorticity with magnitude greater than a specified threshold (generally ~20% of peak jet vorticity). This method worked well for shorter jets. Unit vectors were then computed from the known centerline orientation. (2) Using the angled centerline as the $r$=0 axis, the magnitude of the jet impulse ($I$) and the excess kinetic energy of the jet ($E$) were computed from:

$$I / \rho = \pi \int_{\text{jet}} \omega_\theta \, r^2 \, dr \, dz \, , \qquad (1)$$

$$E / \rho = \pi \int_{\text{jet}} \omega_\theta \psi \, dr \, dz \, , \qquad (2)$$

where $\omega_\theta$ is the azimuthal component of vorticity, $r$ is the radial coordinate relative to the jet centerline, $\psi$ is the Stokes stream function, $z$ is the longitudinal coordinate along the jet axis and $\rho$ is the fluid density. The area integrals were computed using a 2-D version of the trapezoidal rule. The effects of the velocity field around the vortex (not induced by the vortex itself) were considered to have negligible influence on impulse calculations because all vortices considered in our analysis were spaced more than two ring diameters away from other vortices or boundaries. Background flow, i.e. speed of the water in the tunnel, was subtracted out from the flow field so that only excess kinetic energy was measured. (3) The components of the impulse vector in the vertical and horizontal directions were computed based on the direction of $\hat{n}_z$ relative to the horizontal. (4) The length of the jet was computed based on the extent over which the centerline velocity magnitude was above a specified threshold ($L_V$) and the extent over which the jet vorticity field was above a specified magnitude ($L_\omega$). (5) The mean ($U_j$) and peak ($U_{jmax}$) jet velocity along the jet centerline were computed. (6) The jet diameter ($D_\omega$) was determined based on the distance between vorticity peaks perpendicular to the jet centerline.

After computation of the jet parameters listed above, $I$, $D_\omega$, $L_V$ and $L_\omega$ were overlaid on a vorticity plot of the data, allowing the user to visually check the data and allow for the correction of input parameters as necessary. Mean values for $D_\omega$, $L_V$ and $L_\omega$ were computed for the jet sequence and these mean values are presented in the remainder of the paper.

Propulsive jet efficiency ($\eta_P$) was computed using the equation (Lighthill, 1960):

$$\eta_P = \frac{\bar{F}_T U}{\bar{F}_T U + \bar{\dot{E}}} \, , \qquad (3)$$

where $\bar{F}_T$ is the time-averaged jet thrust, $U$ is the mean swimming speed and $\bar{\dot{E}}$ is the time-averaged rate at which excess kinetic energy was shed by the jet. $\bar{F}_T$ was the horizontal component of impulse averaged over several frames after jet termination divided by the total jet cycle period, and $\bar{\dot{E}}$ was the peak excess kinetic energy measurement after jet termination, i.e. kinetic energy remaining after the background flow had been removed, within the sequence of frames divided by the jet cycle period.

## RESULTS
### Jet properties and modes
In this study, Reynolds numbers of the jet ($Re_{jet}$)=200–2000 and Reynolds numbers of the squid ($Re_{squid}$)=1000–16,000 were considered. Over this $Re$ range, jet angle decreased with increased

swimming speed for the five size classes considered (linear regression: d.f.=1, 57, $F$=16.102, $P$<0.001, $R^2$=0.226) (Fig. 1A). Mean jet angles were 37.0±6.53 deg. (±s.d.) for the 3.0–3.9 cm $DML$ size class, 40.6±13.61 deg. (±s.d.) for the 4.0–4.9 cm $DML$ size class, 34.3±8.09 deg. (±s.d.) for the 5.0–5.9 cm $DML$ size class, 28.0±8.47 deg. (±s.d.) for the 6.0–6.9 cm $DML$ size class and 37.9±9.40 deg. (±s.d.) for ≥7 cm $DML$ size class. The ratio of the horizontal component of mean jet velocity ($U_{jx}$) to $U$ decreased with increased swimming speed for the five size classes (power regression for $U_{jx}/U$: d.f.=1, 57, $F$=17.819, $P$<0.001; $R^2$=0.238) (Fig. 1B). Slip, i.e. $U_{jx}/U$ differed significantly with size class (1-factor ANOVA ($U_{jx}/U$): size class: d.f.=4, 54, $F$=5.683, $P$=0.002). Tukey HSD *post hoc* tests revealed that size classes ≥5 cm $DML$ had significantly lower slip ($U_{jx}/U$) than size classes <5 cm $DML$ (Fig. 1C). The horizontal component of mean jet velocity ($U_{jx}$) increased with increased $U$ (linear regression: d.f.=1, 57, $F$=19.786, $P$<0.001, $R^2$=0.258) (Fig. 1D).

Variations in jet structure were observed across all size ranges to some degree, with a continuum from shorter to longer jets being observed (Figs 2–4). However, most of these jet structures could be classified as variations of two jet modes: (1) jet mode I, where the ejected fluid rolled up into an isolated vortex ring (Fig. 2 represents variations of this mode); and (2) jet mode II, where the ejected fluid developed into a leading vortex ring that separated or 'pinched off' from a long trailing jet (Figs 3 and 4 represent variations of this mode). These two jet modes were clearly the most abundant modes observed in *L. brevis,* and both modes were consistently detected in each size class (Figs 5 and 6). Only those jets that could be clearly identified either as jet mode I or jet mode II, like those depicted in Figs 5 and 6, were considered for detailed kinematic, propulsive efficiency and jet property analyses, as mentioned in the Materials and methods.

The ratio of jet length based on the vorticity extent ($L_\omega$) to jet diameter based on peak vorticity locations ($D_\omega$) was <3.0 for jet mode I and >3.0 for jet mode II. The mean ratio of $L_V$ to maximum funnel diameter ($D_{Fmax}$) for jet mode I was 6.24±2.52 (±s.d.) with a range of 3.23–11.45, and the mean $L_V/D_{Fmax}$ ratio for jet mode II was 14.64±4.27 (±s.d.) with a range of 5.89–23.19. Moreover, mean $U_{jx}/U$, $U_j/U$ and $U_{jmax}/U$ were 1.66±0.42 (±s.d.), 1.75±0.61 (±s.d.) and 2.34±1.00 (±s.d.), respectively, for jet mode I and 2.26±0.76 (±s.d.), 2.66±1.20 (±s.d.) and 3.93±1.88 (±s.d.), respectively, for jet mode II. $L_\omega/D_\omega$ increased with increased $U_{jx}/U$ for jet mode II (linear regression: d.f.=1, 27, $F$=8.583, $P$=0.007, $R^2$=0.241) (Fig. 7A) but not for jet mode I (linear regression: d.f.=1, 28, $F$=0.028, $P$=0.869).

*L. brevis* either used jet mode I or jet mode II exclusively while maintaining position against a current within the water tunnel or employed a combination of the two modes (or slight variations of the two modes as illustrated in Figs 2–4). No dependence of $L_\omega/D_\omega$ on swimming speed was detected in this study (linear regression: d.f.=1, 57, $F$=3.817, $P$=0.071), and there was no obvious swimming speed preference for the two jet modes (Fig. 7B). Total jet period (contraction and refilling phase) was significantly lower for jet mode I [mean=0.62±0.06 s (±s.d.)] than for jet mode II [mean=0.70±0.04 s (±s.d.)] [two-tailed paired *t*-test (pairs assigned according to speed and size class), $P$=0.018]. Moreover, jet cycle period (contraction and refilling phase) decreased with increased speed for jet mode I (linear regression: d.f.=1, 28, $F$=36.365, $P$<0.001, $R^2$=0.547) but jet cycle period increased with increased speed for jet mode II (linear regression: d.f.=1, 27, $F$=8.562, $P$=0.007, $R^2$=0.241) (Fig. 7C,D). Fin beat frequency was significantly greater during jet mode I [mean=2.23±0.42 beats s$^{-1}$ (±s.d.)] than jet mode II [mean= 1.51±0.54 beats s$^{-1}$ (±s.d.)] (two-tailed *t*-test, $P$=0.003). Furthermore,
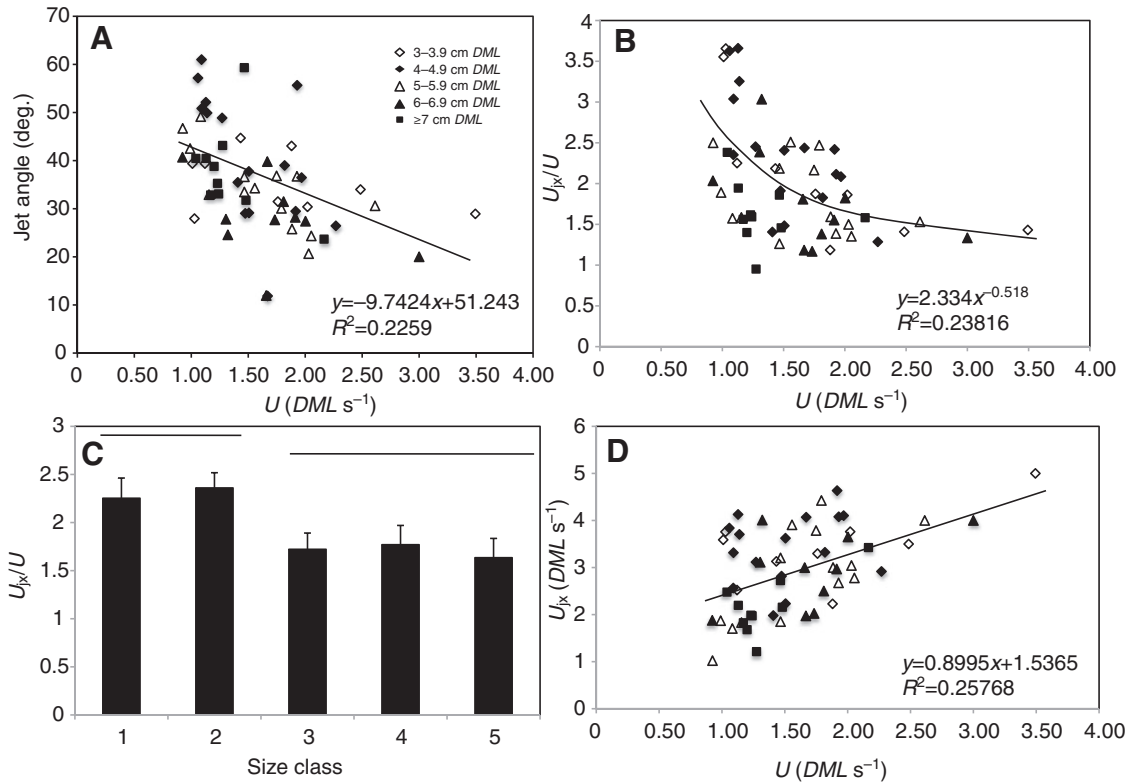
Fig. 1. Jet angle plotted as a function of swimming speed ($U$) (A). Ratio of the horizontal component of mean jet velocity ($U_{jx}$) to $U$ ($U_{jx}/U$) plotted as a function of $U$ (B). $U_{jx}/U$ plotted as a function of size class (C), and $U_{jx}$ plotted as a function of $U$ (D) for juvenile and adult *Lolliguncula brevis*. Size class 1: 3–3.9 cm *DML*, size class 2: 4–4.9 cm *DML*, size class 3: 5–5.9 cm *DML*, size class 4: 6–6.9 cm *DML*, size class 5: ≥7 cm *DML*. Error bars denote ±1 s.e.m.

the two highest speeds where jet mode I was employed (2.6 and 3.5 $DML\,s^{-1}$) involved the highest recorded fin beat frequencies (>3 beats $s^{-1}$).

Over the 248 jet sequences considered, jet mode II was employed more frequently in all size classes but there was relatively greater reliance on jet mode I for size classes <5 cm *DML* than in larger size classes (Fig. 8A). Jet mode II produced significantly more time-averaged thrust and lift than jet mode I, and squid in the largest size class (≥7 cm *DML*) produced significantly more time-averaged lift and thrust than the smallest size class (3–3.9 cm *DML*) (2-factor ANOVA for thrust: jet mode, d.f.=1, 44, $F$=8.687, $P$=0.005; size class, d.f.=4, 44, $F$=3.505, $P$=0.015; 2-factor ANOVA for lift: jet mode, d.f.=1, 44, $F$=7.777, $P$=0.008; size class, d.f.=4, 44, $F$=2.848, $P$=0.035) (Fig. 8B). For size classes ≥5 cm *DML*, thrust production exceeded lift production (paired two tailed *t*-tests, $P$<0.05) but for size classes <5 cm *DML*, lift and thrust production were similar in magnitude (paired two tailed *t*-tests, $P$>0.05) (Fig. 8C).

**Propulsive efficiency**

Although greater time-averaged thrust and lift were produced for jet mode II, jet mode I had higher $\eta_P$ than jet mode II (mean for jet mode I=69±14% (±s.d.) (range: 36–91%), mean for jet mode II=59±14% (±s.d.) (range 27–83%), 2-factor ANOVA (jet mode and size): jet mode factor; d.f.=1, 49, $F$=5.393, $P$=0.020). Squid in the 5–5.9 cm *DML* and 6–6.9 cm *DML* size classes had significantly higher $\eta_P$ than squid in the 4.0–4.9 cm *DML* size class [2-factor ANOVA (jet mode and size): size factor; d.f.=4, 49, $F$=4.753, $P$=0.021] and exhibited a trend in higher $\eta_P$ than the 3–3.9 cm *DML* size class (Fig. 9A). This finding is consistent with the observed reduction in slip for larger size classes, although tempered somewhat

by the lack of higher $\eta_P$ for the largest size class. $\eta_P$ decreased with increased $L_\omega/D_\omega$ (linear regression: d.f.=1, 57, $F$=8.652, $P$=0.005, $R^2$=0.138), which is expected given the observed differences in $\eta_P$ between the two jet modes, and increased with increased $U$ (linear regression: d.f.=1, 57, $F$=18.618, $P$<0.001, $R^2$=0.246) (Fig. 9B,C).

**DISCUSSION**
**Jet modes**

The results from this research together with those of our previous research (Bartol et al., 2009) represent the first comprehensive data set on jet dynamics during ontogeny in squids, providing both global quantification of jet flows and direct measures of propulsive efficiency as a function of life history stage. The present study revealed that juvenile and adult squid are capable of producing several different types of jet flow patterns but that two principal jet 'modes' occur, each with significantly different force production and propulsive efficiency: jet mode I, where the ejected fluid rolled up into an isolated vortex ring, and jet mode II, where the ejected fluid developed into a leading vortex ring that 'pinched off' from a long trailing jet.

The similarities between the jet modes observed in squid and flows produced from mechanically pulsed jets are compelling. In numerous experimental and numerical studies of mechanically generated jet pulses, vortex rings are prevalent, existing as isolated structures during short jets ($L/D \leq F \sim 4$) and as a leading component that pinches off from the trailing jet during long jets ($L/D > F$) (Gharib et al., 1998; Rosenfeld et al., 1998; Mohseni et al., 2001; Krueger et al., 2003; Krueger et al., 2006). These patterns were also observed in juvenile and adult *L. brevis*. As mentioned earlier, there is a physical limit to the size of the vortex ring during pulsed jet ejection,
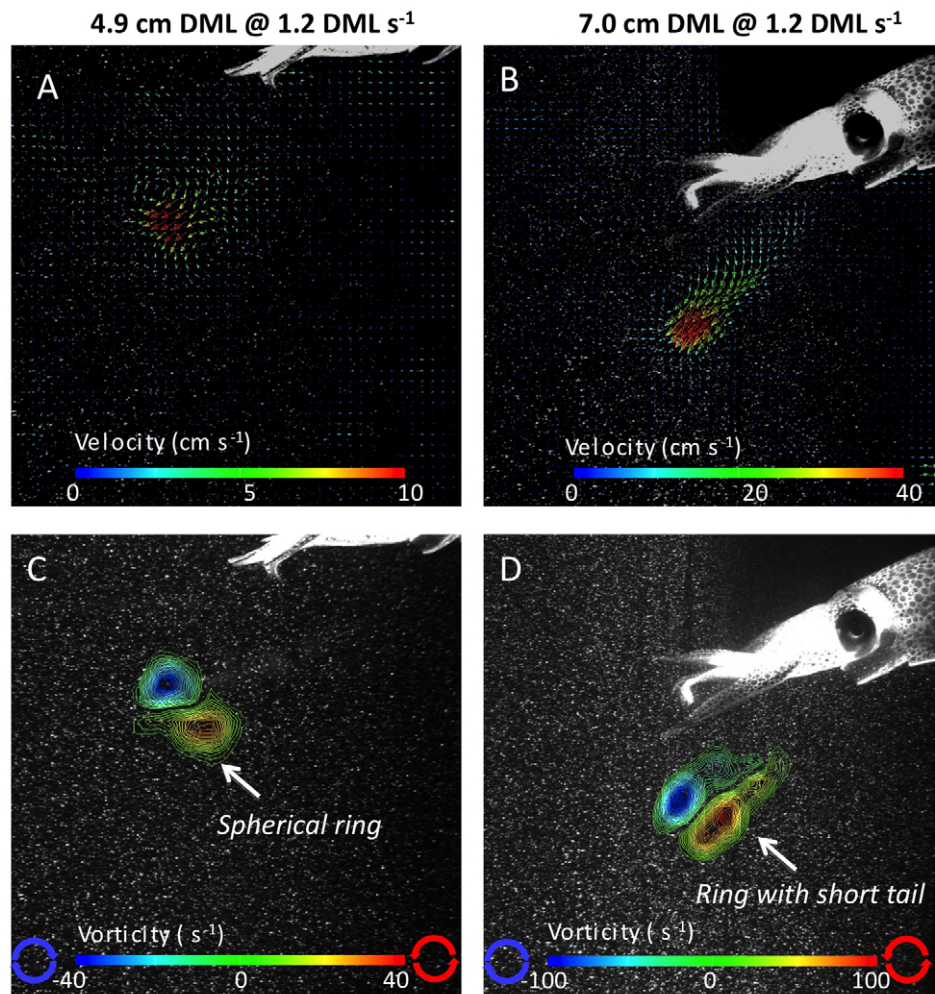
Fig. 2. Velocity (A,B) and vorticity (C,D) fields of isolated vortex rings and vortex rings with short tails observed in a 4.9 cm and 7.0 cm dorsal mantle length (*DML*) *Lolliguncula brevis* swimming at 1.2 *DML* s⁻¹. These jet patterns are classified as jet mode I, where a spherical or elongated vortex ring develops with each jet pulse. All velocity fields have background flow (water tunnel flows) subtracted out, and the red and blue regions denote counterclockwise and clockwise rotation, respectively.

defined in terms of $F$; when $F$ is reached the vortex ring stops entraining circulation, impulse and energy from the generating jet and separates from the jet. Although squid jets have considerable inherent variability and are generated under slightly different conditions than mechanically generated jets (squid jets are inclined relative to the background flow and the funnel aperture is dynamic), the qualitative similarity between jet mode II and classical vortex ring pinch-off indicates the same vortex maximization principle is at work in these flows. Quantitatively, jet mode I was observed for low values (<3) of the ratio of jet length based on vorticity extent ($L_\omega$) to jet diameter based on vorticity peak locations ($D_\omega$). Similarly, jet mode II was observed for $L_\omega/D_\omega>3$. These values are in rough agreement with observations from mechanically generated jets issuing into quiescent fluid where $F\sim4$ (Gharib et al., 1998).

The observation that *L. brevis* can produce jets near $F$ is significant. Studies of mechanically generated jet pulses have demonstrated an optimum in pulse-averaged thrust generated during jet ejection for jet pulses of dimensionless size (duration) close to $F$, i.e. jets near $F$ can produce more thrust per unit of expelled fluid volume than longer duration jets (Krueger and Gharib, 2003). This thrust augmentation benefit, which originates from a higher relative contribution of over-pressure to total impulse at the jet orifice, can be exploited by *L. brevis* given their jet hydrodynamics, although this benefit was not addressed directly in the present study where propulsive efficiency was the focus. Propulsive efficiency measurements indicate that *L. brevis* can produce short jets of high

efficiency, providing the first direct evidence that short jet pulses resulting in isolated vortex rings with no trailing jet (jet mode I) are more efficient than long jet pulses (jet mode II).

Short pulses (with short jet periods) have the advantage that a larger portion of the impulse they generate is related to over-pressure at the nozzle exit plane (Krueger and Gharib, 2003), which is consistent with the observed lower slip for jet mode I relative to jet mode II. Based on the over-pressure benefits one might hypothesize that propulsion by isolated vortex rings would be more efficient but the over-pressure also leads to more kinetic energy in the flow (in the case of static jets) (Krueger, 2001; Choutapalli, 2006), so it is not clear whether the impulse benefit outweighs the kinetic energy cost. Testing on a self-propelled platform is required to determine whether over-pressure improves or degrades propulsive efficiency. The results from the present study provide the first validation of this prediction in a self-propelled system, i.e. squid.

The conclusion that jet mode I is more efficient than jet mode II is tempered somewhat by the observation that fins are more active when jet mode I is being used, suggesting that the fins are providing a larger fraction of the thrust when isolated rings are produced. The fin activity could be artificially inflating the efficiency of jet mode I by increasing $U$ above what it would be normally if only the jet was active. It seems unlikely that this would account for all of the gains for jet mode I, however. First, one cooperative squid employed both jet modes at a particular speed with similar fin contributions. This squid produced propulsive efficiencies of 91% and 75% for

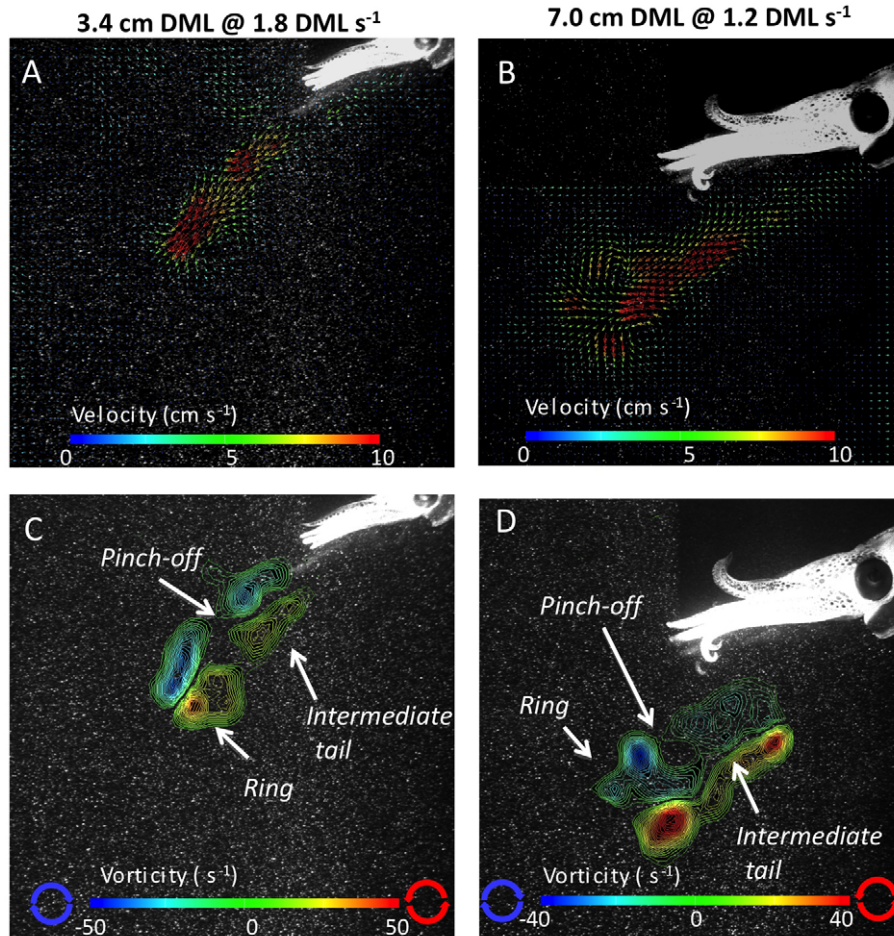**3.4 cm DML @ 1.8 DML s⁻¹**

**7.0 cm DML @ 1.2 DML s⁻¹**



Fig. 3. Velocity (A,B) and vorticity (C,D) fields of leading vortex rings with evidence of pinch-off from an intermediate tail observed in a 3.4 cm and 7.0 cm dorsal mantle length (*DML*) *Lolliguncula brevis* swimming at 1.8 *DML* s⁻¹ and 1.2 *DML* s⁻¹, respectively. These jet patterns are classified as variations of jet mode II, where a vortex ring pinches off from a trailing jet. All velocity fields have background flow (water tunnel flows) subtracted out, and the red and blue regions denote counterclockwise and clockwise rotation, respectively.

jet mode I and jet mode II, respectively. Second, paralarvae enjoy elevated propulsive efficiency from short pulses and their fins appear to have negligible influence on propulsive performance (Bartol et al., 2009). Third, recent studies on a mechanical self-propelled jet vehicle, known as Robosquid, revealed that pulsed jet efficiency increases as the $L/D$ drops below the transition between isolated vortex rings formed with each pulse and leading vortex rings followed by trailing jets (Nichols et al., 2008).

Although vortex rings, both in their isolated form and as the leading component of longer jets, were prominent features in jet flows of juvenile and adult *L. brevis*, this may not be true for other adult squids. In adult long-finned squid *D. pealeii* (~27 cm *DML*), Anderson and Grosenbaugh (Anderson and Grosenbaugh, 2005) mostly observed periodic prolonged emissions of fluid without defined leading vortex rings during jetting, and they did not detect steady propulsion by individual vortex rings, as was the case in the present study. Anderson and Grosenbaugh (Anderson and Grosenbaugh, 2005) discuss the important effects of background flow on jet structure, arguing that vortex ring formation should become less prominent as background flow velocity, i.e. swimming velocity, approaches jet velocity. Moreover, as was the case with Krueger et al. (Krueger et al., 2003), Anderson and Grosenbaugh observed a decrease in $F$ in pipe jet experiments when jet velocities were less than twice background flow velocity (i.e. swimming speed) (see Anderson and Grosenbaugh, 2005). As noted by Krueger et al. (Krueger et al., 2003), some decrease in $F$ with increased co-flow may be expected given that a higher co-flow component decreases the strength of the shear layer feeding the ring while increasing the

rate of advection of the ring away from the nozzle, limiting the growth of the leading vortex ring. Anderson and Grosenbaugh (Anderson and Grosenbaugh, 2005) reported jet velocities of 1.4–4.5 times the swimming speed in *D. pealeii*, with lower values occurring at the highest swimming speeds. In the present study, mean $U_{jx}/U$, $U_j/U$ and $U_{jmax}/U$ ranged from 1.1 to 3.7, 1.2 to 5.5 and 1.4 to 7.6, respectively, across size classes. Direct comparison of the jet structures produced by *L. brevis* and *D. pealeii* is not possible because of the different swimming *Re* ranges considered (1000–16,000 for *L. brevis*, 22,000–180,000 for *D. pealeii*). However, it is interesting that only sporadic/reduced vortex ring formation was observed in *D. pealeii* adults even though similar jet speed/swimming speed ratios were observed in both squids.

In addition to interspecific distinctions in jet structure, there are also important ontogenetic differences. In contrast to adult *D. pealeii*, paralarval *D. pealeii* produce a continuum of vortex ring structures from classical spherical rings to 'elongated vortex rings', i.e. flows with higher aspect ratios than conventional vortex puffs but lower aspect ratios than prolonged emissions of fluid generally associated with a jet (Bartol et al., 2009). Despite producing jets with $L_\omega/D_\omega>3$, pinch-off was not clearly observed in *D. pealeii* hatchlings, distinguishing paralarval jet wakes from those observed in the present study. The authors hypothesized that the absence of pinch-off was a product of viscous diffusion either (1) obscuring leading ring separation from a trailing jet or (2) preempting complete vortex ring formation, resulting in the presence of a vortical tail. Considered collectively, the findings of Bartol et al. (Bartol et al., 2009), Anderson and Grosenbaugh (Anderson and Grosenbaugh, 2005),

**5.3 cm DML @ 2.0 DML s⁻¹**

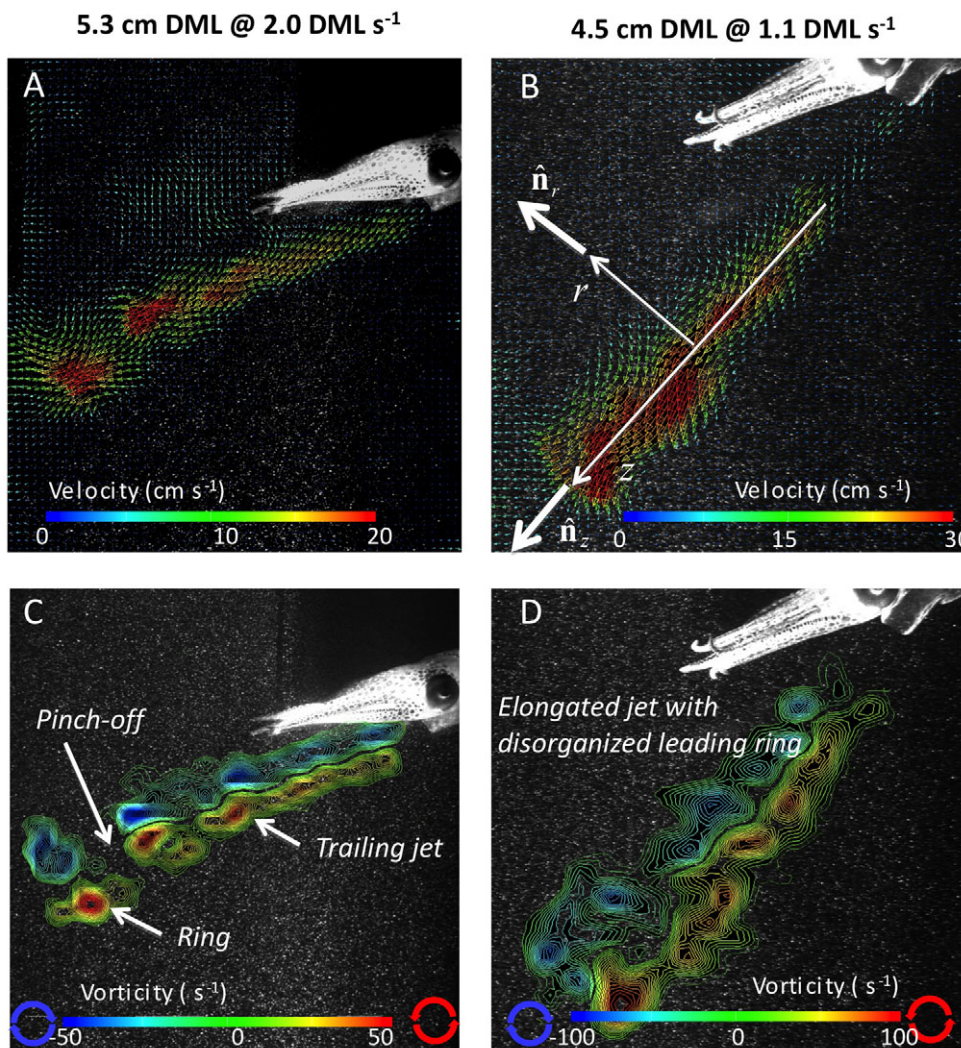**4.5 cm DML @ 1.1 DML s⁻¹**



Fig. 4. Velocity (A,B) and vorticity (C,D) fields of leading vortex rings with evidence of pinch-off from a long tail observed in a 5.3 cm and 4.5 cm dorsal mantle length (*DML*) *Lolliguncula brevis* swimming at 2.0 *DML* s⁻¹ and 1.1 *DML* s⁻¹, respectively. These jet patterns are classified as variations of jet mode II, where a vortex ring pinches off from a trailing jet. In D, the leading ring is disorganized as the flow has become highly asymmetric. All velocity fields have background flow (water tunnel flows) subtracted out, and the red and blue regions denote counterclockwise and clockwise rotation, respectively. In B, $z$ is the longitudinal coordinate along the jet axis, $r$ is the radial coordinate relative to the jet centerline, $\hat{n}_r$ is the unit vector in the radial direction relative to the jet centerline and $\hat{n}_z$ is the unit vector in the longitudinal direction along the jet centerline.

and the present study indicate scale impacts jet structure, with (1) vortex rings and elongated vortex rings forming at small sizes (~0.18 cm *DML* in *D. pealeii* hatchlings), (2) vortex rings and leading vortex rings with trailing jets forming at intermediate sizes (~3–9 cm *DML* in *L. brevis*), and (3) elongated emissions of fluid with instability waves in the jet shear layer forming at larger sizes (~22–30 cm *DML* in *D. pealeii* adults).

### Gaits

According to Alexander, a gait is defined as a 'pattern of locomotion characteristics of a limited range of speeds described by quantities of which one or more change discontinuously at transitions to other gaits' (Alexander, 1989). Gaits have been widely reported in flyers (Spedding et al., 1984; Rayner, 1985; Alexander, 1986; Alexander, 2003; Hedrick et al., 2002; Spedding et al., 2003), swimmers (Webb, 1971; Hove et al., 2001; Korsmeyer et al., 2002) and walkers/runners (Cavagna and Zamboni, 1976; Cavagna et al., 1977; Alexander, 1977; McMahon and Greene, 1979; Biewener, 1983; Hildebrand, 1989; Biewener and Taylor, 1986; Gillis and Biewener, 2001; Robilliard et al., 2007). Gaits are particularly important for nektonic organisms because mechanical power requirements increase with swimming speed raised to the third power and a single motor system is generally insufficient to provide efficient power over a nekton's wide speed and acceleration ranges (Webb, 1994; Webb, 2006).

Consequently, nekton often employ discrete locomotor patterns, i.e. gears or gaits, as needed to provide requisite power, often at high muscle efficiency, as speed increases. Not surprisingly, gaits and gait transitions in aquatic locomotors are often defined according to muscle recruitment and/or kinematic parameters (Blake, 1978; Webb, 1993; Webb, 1994; Webb, 1998; Rome, 1994; Drucker and Jensen, 1996; Webb and Gerstner, 2000; Hove et al., 2001) whereas some gait transitions are described as a function of fluid constraints and thrust production (Seibel et al., 1998; Childress and Dudley, 2004). With the advent of DPIV in recent years, new gait categories have been established according to qualitative wake features in different species of fishes (see Drucker and Lauder, 1999; Wilga and Lauder, 2004; Lauder and Tytell, 2006).

Previous studies have reported 'gaits' or 'behavioral transitions' in squid based largely on kinematic patterns. In one *Doryteuthis* (formerly *Loligo*) *opalescens* (*DML*, 13.5 cm), O'Dor (O'Dor, 1988) identified four gaits: (1) gait 1 occurred at 10 cm s⁻¹ and was characterized by small amplitude mantle contractions and 2 fins beats s⁻¹; (2) gait 2 occurred at 20–40 cm s⁻¹ and involved intermediate amplitude mantle contractions and 1 fin beat s⁻¹; (3) gait 3 occurred at 50 cm s⁻¹ and involved large amplitude mantle contractions and no fin beats; and (4) gait 4 occurred at 1.4 m s⁻¹ (escape jet speeds) and was characterized by maximal amplitude mantle contraction, a long contraction phase and no fin beats. Bartol
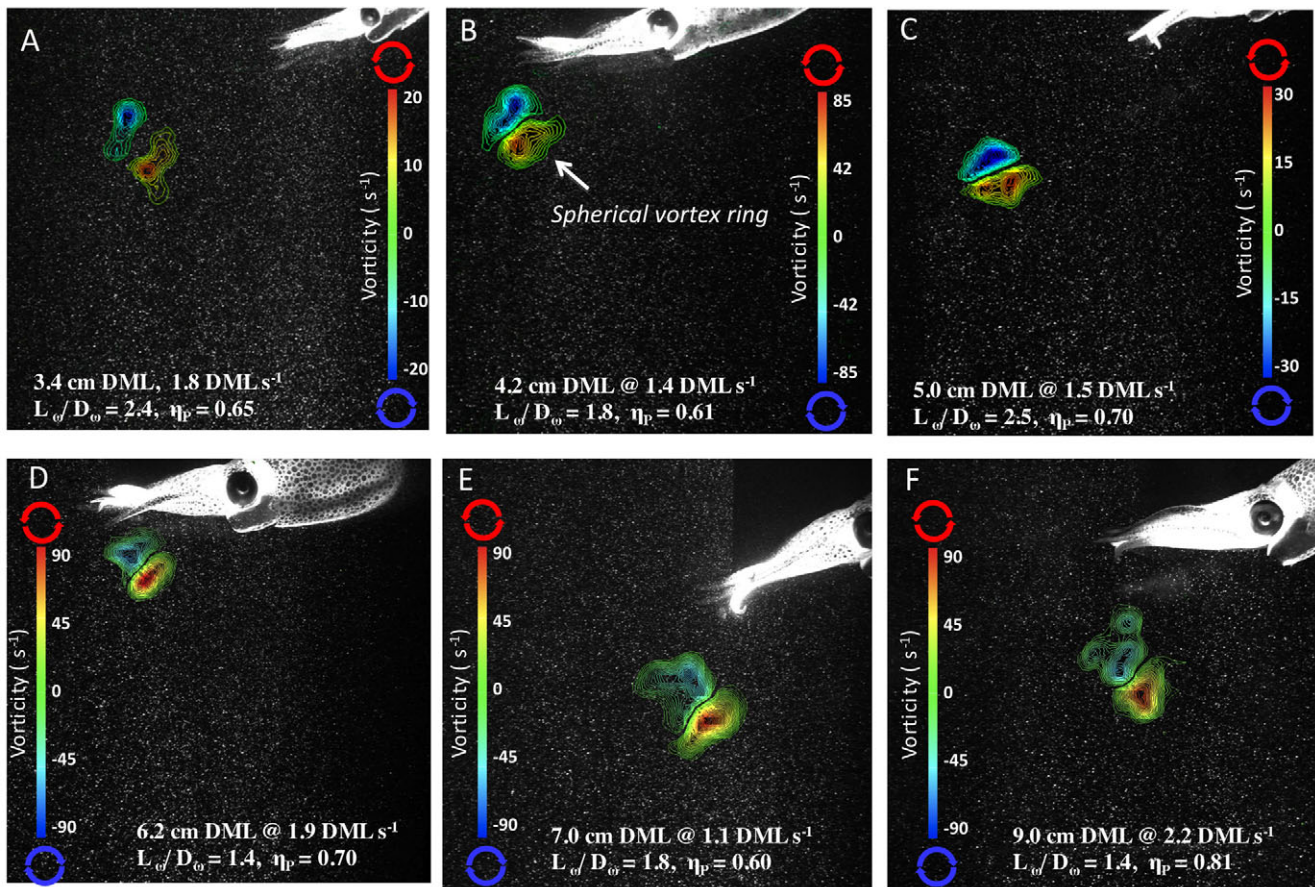
Fig. 5. Vorticity contour fields for six brief squid *Lolliguncula brevis* [3.4–9.0 cm dorsal mantle length (*DML*)] swimming at speeds from 1.1–2.2 $DML\,s^{-1}$ and producing vortex rings, i.e. jet mode I ($L_\omega/D_\omega<3$). Red and blue regions denote counterclockwise and clockwise rotation, respectively. $L_\omega/D_\omega$ and propulsive efficiency ($\eta_P$) are mean values for the entire jet cycle. $L_\omega$ is the jet length based on the vorticity extent; and $D_\omega$ is the distance between vorticity peaks.

et al. observed more gradual kinematic transitions in *L. brevis* during steady swimming speeds (escape jets were not considered), with mantle amplitude generally increasing and fin activity generally decreasing with speed in squid 3.0–8.9 cm *DML* (Bartol et al., 2001b). A notable exception to these trends was *L. brevis* 1.0–2.9 cm in *DML*. These early juvenile squid exhibited an abrupt drop in fin beat frequency from 2 Hz at a swimming speed of 9 cm s$^{-1}$ to 0 Hz at 12 cm s$^{-1}$ and increased mantle pulsing frequency with swimming speed, all while maintaining relatively constant mantle contraction amplitude. The finding of Bartol et al. (Bartol et al., 2001b) that *L. brevis* 3.0–8.9 cm *DML* do not demonstrate a significant increase in mantle pulsing frequency with swimming speed makes sense in the context of the two jet modes observed in the present study. Over the speed range of ~1–3 $DML\,s^{-1}$, *L. brevis* employed both jet mode I and jet mode II, with jet mode I showing a decrease in jet period with speed and jet mode II showing an increase in jet period with speed. These conflicting jet period relationships preclude detection of consistent trends in mantle contraction frequency with speed when jet mode is unknown.

The present study is the first to identify different hydrodynamic jet 'modes' in squid, each with significantly different propulsive efficiency, force production and jet periods. Although previous analyses performed on a limited number of *L. brevis* indicated that jet mode I was used more often at low speeds (i.e. <1.5 $DML\,s^{-1}$) and jet mode II was employed more often at high speeds (i.e. >1.5 $DML\,s^{-1}$) (Bartol et al., 2008), the more expansive data set considered in the

present study does not support this trend. The lack of speed dependence on jet mode was unexpected, especially considering the observed difference in overall force production between the jet modes.

The absence of a dependence of jet mode on speed may be a product of the narrow speed range considered (~1–2.25 $DML\,s^{-1}$ for most of the data). Two types of circular muscles drive mantle contraction: centrally located mitochondria-poor (CMP) fibers and superficially located mitochondria-rich (SMR) fibers (Bone et al., 1981; Mommsen et al., 1981) [see terminology from Preuss et al. (Preuss et al., 1997)]. SMR fibers have greater thick filament lengths, lower maximum unloaded shortening velocity and higher peak isometric stress than CMP fibers (Thompson and Kier, 2006; Thompson et al., 2008). These two types of circular muscle fibers are electrically active at different swimming speeds. In an earlier study, Bartol correlated mantle kinematics with electromyography (EMG) records at various swimming speeds and observed SMR electrical activity at low speeds (<1 $DML\,s^{-1}$), sporadic CMP activity at intermediate speeds (1–3 $DML\,s^{-1}$) and full recruitment of CMP fibers at high speeds (>3 $DML\,s^{-1}$) (Bartol, 2001). Based on these previous findings (Bartol, 2001), SMR and CMP fibers – muscle groups most likely to provide power for jet mode I and II, respectively – are used intermittently over the speed range considered in the present study, which is certainly consistent with the observed oscillations between jet modes. If a broader range of speeds was considered, i.e. more speeds <1 and >3 $DML\,s^{-1}$, it is likely that mode preferences would emerge at the extremes of the swimming range
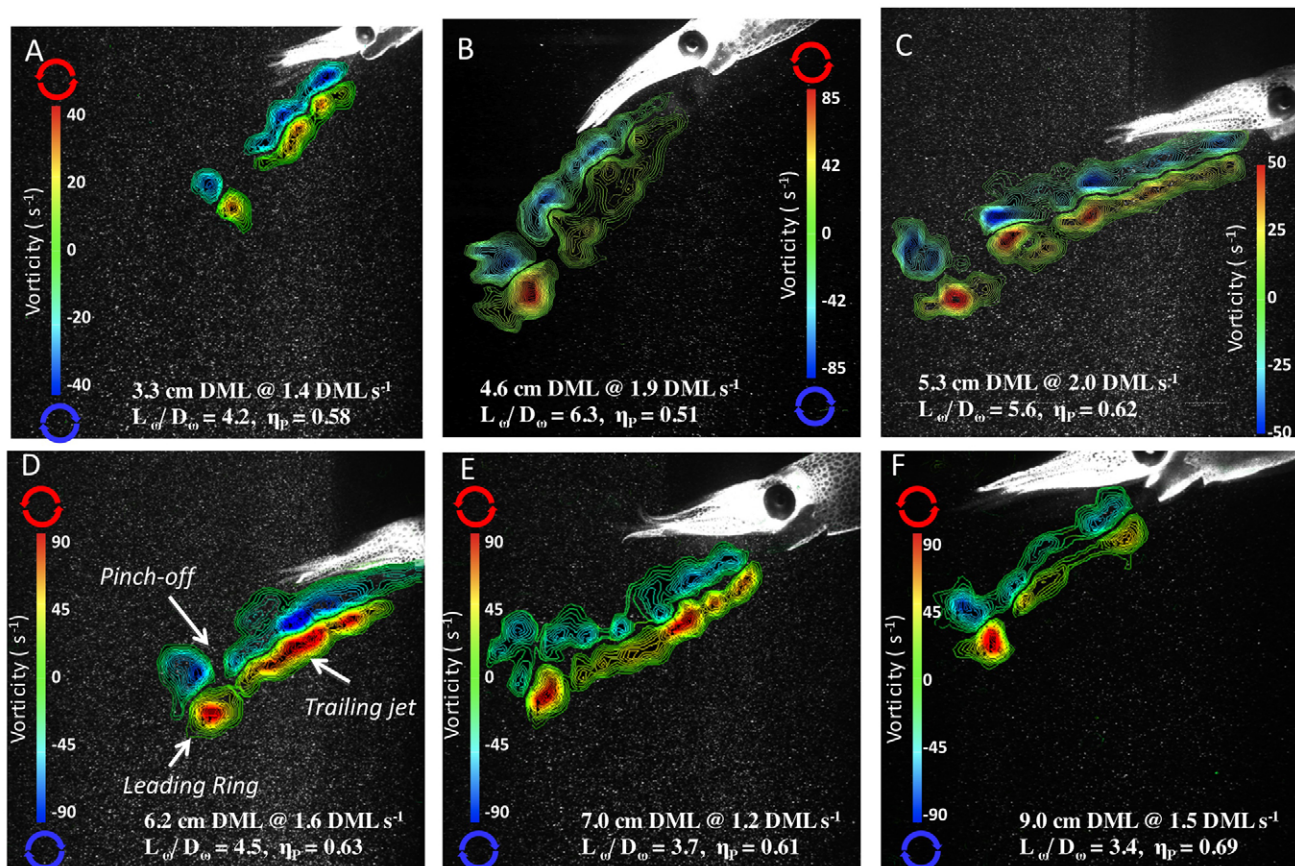
Fig. 6. Vorticity contour fields for six brief squid *Lolliguncula brevis* [3.3–9.0 cm dorsal mantle length (*DML*)] swimming at speeds from 1.2–2.0 *DML* s$^{-1}$ and producing leading vortex rings that pinch off from a trailing jet, i.e. jet mode II ($L_\omega/D_\omega$>3). Red and blue regions denote counterclockwise and clockwise rotation, respectively. $L_\omega/D_\omega$ and propulsive efficiency ($\eta_P$) are mean values for the entire jet cycle. $L_\omega$ is the jet length based on the vorticity extent; and $D_\omega$ is the distance between vorticity peaks.

where SMR and CMP fibers are used more exclusively. Not only does the intermittent use of the muscle groups and modes provide greater locomotive flexibility, it also presumably contributes to lower metabolic swimming costs and reduced build-up of anaerobic end products in *L. brevis* (see Finke et al., 1996; Bartol et al., 2001a).

Fin activity may have played a role in extending the speed range over which jet mode I was employed, making it difficult to identify a clear shift in jet modes as a function of speed. Bartol et al. found that *L. brevis*, in the size range considered for this study, generally terminate fin activity at speeds >2.5 *DML* s$^{-1}$ (Bartol et al., 2001b). As the majority of the speeds considered in the present study were <2.5 *DML* s$^{-1}$, the fins were active (as evident in kinematic footage) and were producing propulsive forces based on the findings of W.J.S., I.K.B. and P.S.K. (in preparation), who observed significant thrust production by the fins within the speed range considered here. Based on this force production, it is likely that the fins expanded the speed range for jet mode I beyond what it would have been without fin input. In the absence of fin activity, mantle contraction frequency has to increase with speed to provide the requisite lift and thrust forces from an isolated vortex ring structure. Based on the observed decrease in jet period with speed for jet mode I, it is clear that *L. brevis* use this approach, even when the fins are active. Eventually contraction frequency will reach a limit, however, which is determined by: (1) elastic properties of the mantle tissue; (2) shortening velocities of radial muscles during refilling; (3) the mechanical properties of the mantle circular muscles; and (4)

nervous system control over circular muscle activation (Bone et al., 1981; Mommsen et al., 1981; Gosline et al., 1983; Gosline and Shadwick, 1983; Otis and Gilly, 1990; Gilly et al., 1991; MacGillivray et al., 1999; Thompson and Kier, 2001; Thompson and Kier, 2002; Thompson and Kier, 2006; Thompson et al., 2008). When the contraction frequency limit is reached while jet mode I is employed, fin activity will have to meet the added force demands. Therefore, fin behavior (i.e. frequency, amplitude, mode, etc.) may be more relevant than speed in determining which jet mode is selected for the range of speeds considered in the present study. Coupling jet mode I with high fin activity is a reasonable strategy given the propulsive efficiency benefits afforded by both short pulses and fin motion – a component of the propulsive system with even higher propulsive efficiency than the jet (see Bartol et al., 2008).

With the lack of a consistent dependence of jet mode on speed, jet mode I and II do not fall within the purview of classical 'gaits' as defined by Alexander (Alexander, 1989). Given the dual mode propulsive system of squids, both the jet and the fins need to be considered for proper identification of gaits (and probably a wider speed range). In fact, up to four potential fin modes occur in *L. brevis*, some of which have overlapping speed ranges like the jet modes described in the present study (W.J.S., I.K.B. and P.S.K., in preparation). Although beyond the scope of the present paper, the complex coordination and synergistic hydrodynamic effects of these various jet and fin modes is essential for sufficient identification of classical gaits.
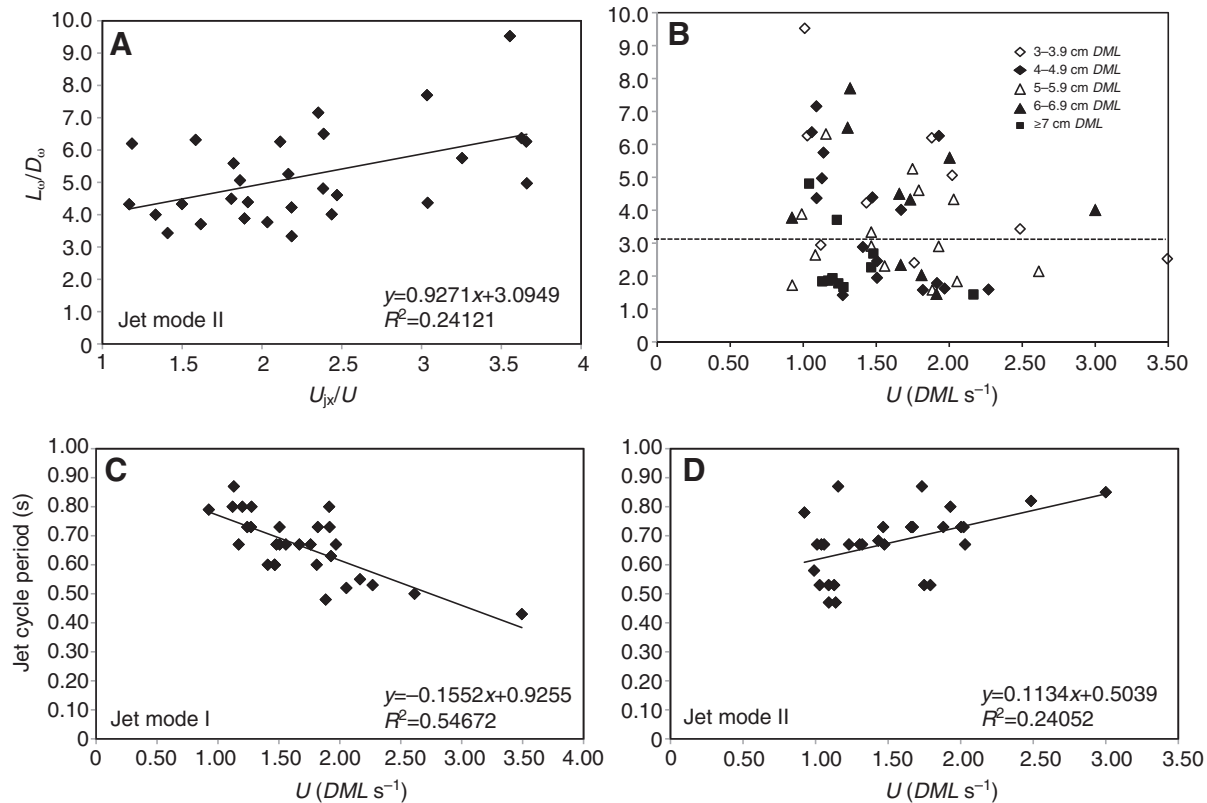
Fig. 7. $L_\omega/D_\omega$ plotted as a function of slip ($U_{jx}/U$) for jet mode II (A), $L_\omega/D_\omega$ plotted as a function of swimming speed ($U$) (B), jet cycle period plotted as a function of $U$ for jet mode I (C) and jet cycle period plotted as a function of $U$ for jet mode II (D). In B, the dotted line represents the demarcation between vortex rings (jet mode I) and vortex rings with a trailing jet (jet mode II). $L_\omega$ is the jet length based on the vorticity extent; $D_\omega$ is the distance between vorticity peaks; and $U_{jx}$ is the horizontal component of mean jet velocity along the jet centerline.

### Jet properties and propulsive efficiency

The observed decrease in jet angle with increased speed is consistent with previous studies on *D. opalescens*, *D. pealeii*, *Illex illecebrosus* and *L. brevis*, which show a decrease in the angle of the funnel, mantle and/or jet with increased speed (O'Dor and Webber, 1986; O'Dor, 1988; Bartol et al., 2001b; Anderson and Grosenbaugh, 2005). Higher jet angles at lower speeds are required for these squids because they are negatively buoyant; thus, they need to direct their jets more vertically to maintain depth at low speeds when dynamic lift forces are low. Directing jets at angles steeply subtended to horizontal coupled with positioning the body at high angles for body lift generation at low speeds leads to high energetic costs (see Bartol et al., 2001a; Bartol et al., 2001b).

In the present study, *L. brevis* also exhibited a significant decrease in slip along with an increase in propulsive efficiency with increased speed, as was also the case with *D. pealeii* paralarvae (Bartol et al., 2009). Using a different approach for calculating propulsive efficiency, Anderson and Grosenbaugh reported similar results in *D. pealeii* and suggested that the efficiency increase was likely to be a result of reduction in the excess kinetic energy in the jet with speed as slip decreases (Anderson and Grosenbaugh, 2005). High propulsive efficiencies ($\geq$78%) coupled with low slip ($\sim$1.3–1.6) at high speeds recorded for *L. brevis* in the present study and *D. pealeii* paralarvae and adults in other studies (Anderson and Grosenbaugh, 2005; Bartol et al., 2009) contradict the presumption that squids have low propulsive efficiency because of a low-volume, high-velocity jet (Alexander, 1968; Lighthill, 1975; Vogel, 2003). Indeed, squid are capable of generating high-volume, low-velocity jets with high propulsive efficiency.

The propulsive efficiency story gets even more intriguing when the different jet modes and $L_\omega/D_\omega$ are considered. Although $L/D$ increases with swimming speed in adult *D. pealeii* (Anderson and Grosenbaugh, 2005) and higher ratios of net-impulse to energy are predicted with increased $L/D$ when background flow is involved (Jiang and Grosenbaugh, 2006), this was not the case for juvenile and adult *L. brevis*. In the present study, no clear relationship between $L_\omega/D_\omega$ and speed was detected, and propulsive efficiency decreased with increased $L_\omega/D_\omega$. These results together with those described in the previous two paragraphs suggest that three factors have an important impact on propulsive jet efficiency: (1) jet angle, (2) slip, and (3) jet mode. At high speeds, jet angle decreases, allowing a higher fraction of the jet impulse to contribute to useful propulsive work, and slip decreases, resulting in less wasted kinetic energy in the wake. The observed decrease in propulsive efficiency with increased $L_\omega/D_\omega$ is expected given the higher propulsive efficiency of jet mode I ($L_\omega/D_\omega<3$) relative to jet mode II ($L_\omega/D_\omega>3$). Therefore, not only are squid capable of generating high efficiency jets at high speeds, when both jet angle and slip are low but some squid, such as juvenile and adult brief squid *Lolliguncula brevis* and paralarval *D. pealeii*, are capable of generating high efficiency short jets that evolve into spherical and elongated vortex rings over a fairly broad range of speeds.

The propulsive jet efficiencies reported in this study [mean $\eta_p$ for jet mode I=69$\pm$14% ($\pm$s.d.) (range: 36–91%); mean for jet mode II=59$\pm$14% ($\pm$s.d.) (range 27–83%)] are lower than those reported in other DPIV studies of jet propulsion. In an earlier study, we observed mean jet propulsive efficiencies of 80.7% and 71.3% for jet mode I and II, respectively (Bartol et al., 2008). However, these
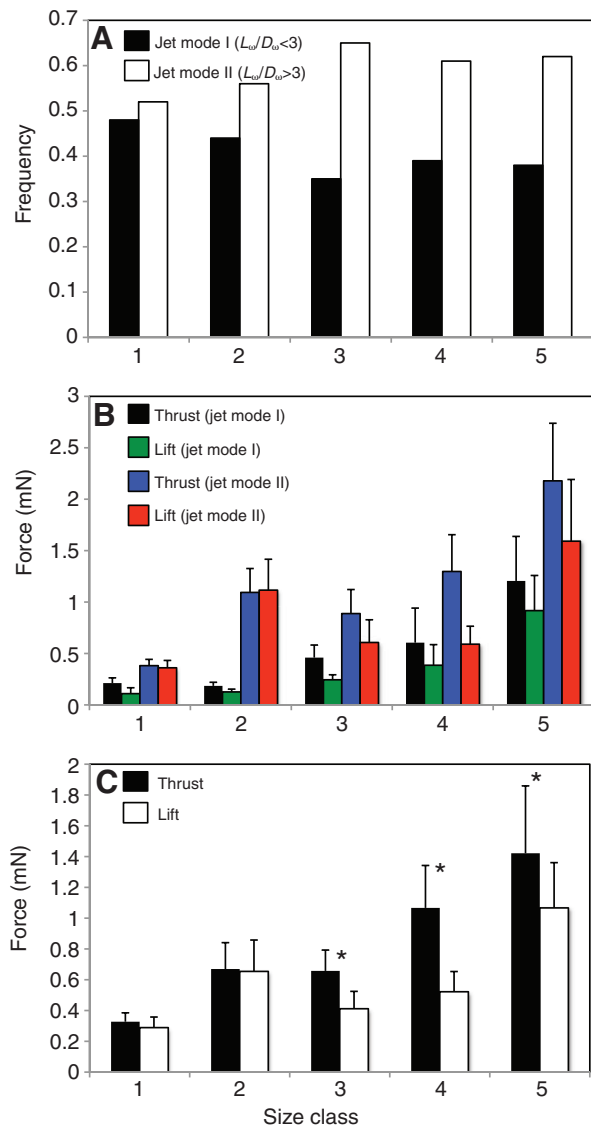
Fig. 8. Frequency of occurrence of jet wakes with $L_\omega/D_\omega < 3$ (jet mode I) and jet wakes with $L_\omega/D_\omega > 3$ (jet mode II) plotted as a function of size class (A); lift and thrust production for brief squid *Lolliguncula brevis* in different size classes when swimming at $1–2\,DML\,s^{-1}$ and producing wakes with $L_\omega/D_\omega < 3$ (jet mode I) and $L_\omega/D_\omega > 3$ (jet mode II) (B); and lift and thrust production (composite for both jet modes) by *L. brevis* of different sizes swimming at speeds of $1–2\,DML\,s^{-1}$ (C). Size class 1: $3–3.9\,cm$ dorsal mantle length (*DML*), size class 2: $4–4.9\,cm\,DML$, size class 3: $5–5.9\,cm\,DML$, size class 4: $6–6.9\,cm\,DML$, and size class 5: $\geq 7\,cm\,DML$. In C, asterisks denote significant differences ($P < 0.05$) between time-averaged lift and thrust. Error bars denote $\pm 1$ s.e.m. $L_\omega$ is the jet length based on the vorticity extent; and $D_\omega$ is the distance between vorticity peaks.

Fig. 9. Propulsive efficiency ($\eta_P$) for jet mode I and II as a function of size class (A), $\eta_P$ *versus* ratio of jet length based on vorticity extent to jet diameter based on the distance between vorticity peaks ($L_\omega/D_\omega$) (B) and $\eta_P$ *versus* swimming speed *(U)* (C) for brief squid *Lolliguncula brevis* [$3.3–9.1\,cm$ dorsal mantle length (*DML*)]. In B, the dotted line represents the demarcation between vortex rings (jet mode I) and vortex rings with a trailing jet (jet mode II). Size class 1: $3–3.9\,cm\,DML$, size class 2: $4–4.9\,cm$ *DML*, size class 3: $5–5.9\,cm\,DML$, size class 4: $6–6.9\,cm\,DML$, size class 5: $\geq 7\,cm\,DML$. Error bars denote $\pm 1$ s.e.m.

mean values, which fall within the ranges reported in the present study, are based on a much smaller sample of data and consequently the means from the present study are more representative of an ontogenetic range of *L. brevis*. Based on the equation for rocket motor propulsive efficiency with adjustments for jet angle, Anderson and Grosenbaugh (Anderson and Grosenbaugh, 2005) calculated jet propulsive efficiency means in adult *D. pealeii* (27 cm *DML*) of 86% for speeds $> 0.65\,DML\,s^{-1}$, which represents ~80% of the speed range, and 93% for speeds $> 1.6\,DML\,s^{-1}$, which represents ~28% of the speed range. Anderson and Grosenbaugh (Anderson and

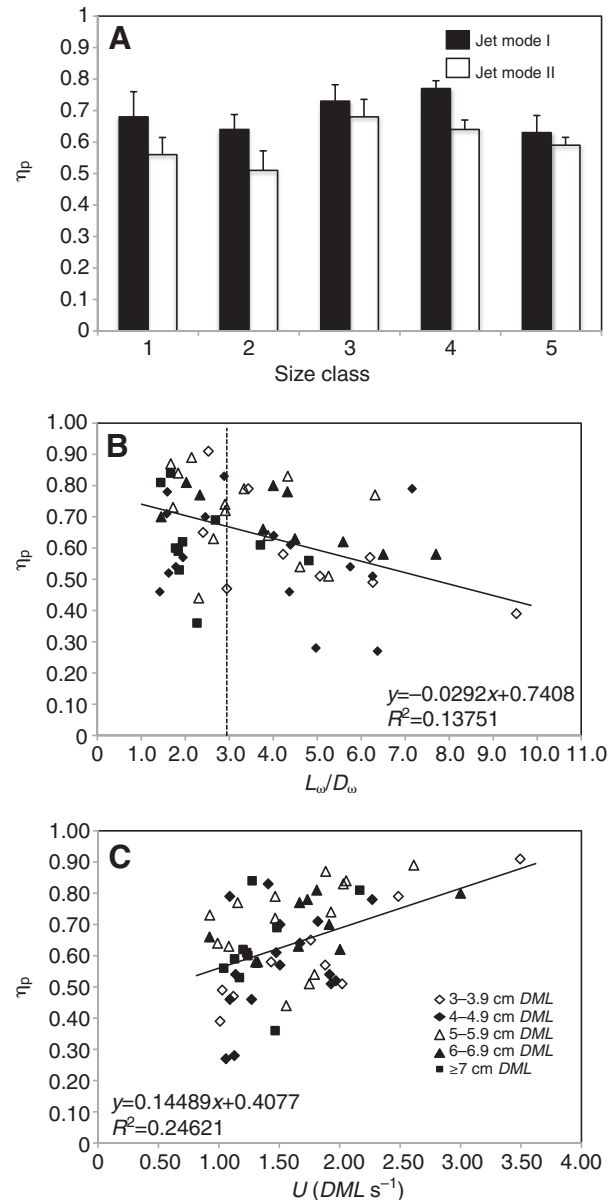Grosenbaugh, 2005) reported that these means are consistent with efficiencies calculated from estimates of total and excess kinetic energy in the jet, but indicated efficiencies based both on kinetic energy and rocket motor equations may be slightly inflated because jet velocities used in the equations could be underestimates of true velocities (the full extent of the jet was often not captured because of a limiting field of view). Although juvenile/adult *L. brevis* differ morphologically, behaviorally and physiologically from adult *D. pealeii*, propulsive efficiencies for similar speed ranges are as follows: 64% for speeds $> 0.65\,DML\,s^{-1}$, which represents 100% of

the speed range considered in the present study; 70% for speeds >1.6 $DML\,s^{-1}$, which represents 38% of the speed range; and 78% for speeds >2 $DML\,s^{-1}$, which represents 22% of the speed range. The overall propulsive efficiency of 64% for the present study is higher than the mean propulsive efficiency of 53.5% reported by Bartol et al. (Bartol et al., 2001b), who used the rocket motor equation for propulsive efficiency, kinematic measurements and jet velocity estimates determined from flow tracer particles. Again, propulsive jet efficiencies reported in the present study are more reliable because they were derived from direct global measurements of bulk properties of the jet flows and they account for jet angle.

One question that remains unresolved in the present study is: why would squid prefer using jet mode II, a mode with less propulsive efficiency than jet mode I? One possibility is that jet mode II allows for the employment of a highly efficient fin 'gait'. Although 3-D kinematics and flow dynamics of the fins were not examined in the present study, the observed difference in fin frequency between the jet modes, coupled with the detection of a wide suite of fin modes in another study (W.J.S., I.K.B. and P.S.K., in preparation) suggests that fin motions may differ markedly in the two jet modes. It is conceivable that jet mode II, which offers higher time-averaged thrust and lift production, allows for a higher amplitude, lower frequency, more efficient fin stroke than is possible with jet mode I. As mentioned earlier, greater force production from the fins is necessary when the requisite pulsing frequencies for lift and thrust production are not attainable in jet mode I. Consequently, jet mode I may require 'force-maximizing' fin gaits as opposed to 'efficiency-maximizing' fins gaits. Similar divisions between stroke types have been observed in birds (Spedding et al., 2003; Alexander, 2002) and fishes (Drucker and Lauder, 2000; Nauen and Lauder, 2002). The efficiency gains of a particular fin gait may indeed outweigh the loss in jet propulsive efficiency associated with jet mode II, resulting in a net propulsive efficiency gain for jet mode II relative to jet mode I. Obviously, many questions remain but clearly hydrodynamic studies of fin and jet coordination are warranted to better understand gait use in squids.

### Ontogenetic differences

Our earlier studies (Bartol et al., 2008; Bartol et al. 2009) provide evidence that paralarvae enjoy higher propulsive efficiency than their juvenile/adult counterparts. Although higher paralarval propulsive efficiency was unexpected, a disparity in propulsive efficiency is not surprising given key differences in morphology (e.g. relative funnel size, mantle musculature, relative fin size) and flow environments ($Re_{squid}$<100 *versus* $Re_{squid}$>1000) between paralarvae and older life stages.

In addition to the ontogenetic transition from paralarvae to older life stages, another important ontogenetic shift for *L. brevis* (in terms of jet dynamics) appears to occur at ~5.0 cm *DML* based on the results of the present study. Significantly lower slip occurred in size classes ≥5.0 cm *DML* than size classes <5.0 cm *DML*, and squid 5.0–6.9 cm had greater propulsive efficiency than size classes <5.0 cm *DML*. Despite having lower slip than size classes <5.0 cm *DML*, squid ≥7 cm *DML* did not have significantly greater propulsive efficiency. This is probably related to the consideration of a higher proportion of low-speed swimming sequences, which involve high jet angles and thus a lower fraction of the jet impulse contributing to useful propulsive work, for squid ≥7.0 cm *DML* relative to other size classes (see Fig. 1A).

While squid in all size classes demonstrated a preference for jet mode II, size classes <5.0 cm *DML* exhibited proportionally greater reliance on jet mode I, the jet mode with the shortest jet cycle period.

This is consistent with the findings of J.T.T., P.S.K. and I.K.B. (in preparation) in that the thick filament lengths of the CMP and SMR circular muscle fibers that provide power for jet locomotion in *D. pealeii* and *Sepioteuthis lessoniana* increase significantly during growth, thereby contributing to an ontogenetic decrease in the rate of mantle contraction during escape jetting.

The higher relative contribution of the jet to lift in *L. brevis* <5.0 cm *DML* is noteworthy for it suggests that squid <5.0 cm *DML* are more negatively buoyant than larger squid and/or produce less lift with their fins. Although paralarval through to adult *L. brevis* are negatively buoyant (Bartol et al., 2001a; Bartol et al., 2001b), a detailed assessment of buoyancy throughout ontogeny has not been performed. Despite biomechanical models for fin function (Kier, 1989; Kier et al., 1989; Johnsen and Kier, 1993), nothing is known of the mechanical properties of the muscle groups of the fins or how those properties may change during ontogeny. Therefore, further examination of buoyancy and fin muscular mechanics is required to fully address the above finding.

### Concluding thoughts

Two distinct jet modes were observed in this study: (1) jet mode I, where the ejected fluid rolled up into an isolated vortex ring with low overall time-averaged force production but high propulsive efficiency; and (2) jet mode II, where the ejected fluid developed into a leading vortex ring that pinched off from a long trailing jet, leading to high time-averaged force production but lower propulsive efficiency. This is the first observation of distinct, quantitatively based, hydrodynamic jet modes in squid, suggesting that certain squid have access to both short pulsed and long pulsed jet strategies. Moreover, this study provides the first confirmation that thrust augmentation known to accompany short jets in tethered conditions (Krueger and Gharib, 2003; Krueger and Gharib, 2005) can also lead to enhanced propulsive efficiency in freely swimming biological jetters. This finding is consistent with parallel studies on mechanical underwater jet-propelled vehicles that also demonstrate enhanced propulsive efficiency from short vortex ring jets (Nichols et al., 2008). In addition to jet mode and $L_{\omega}/D_{\omega}$, jet propulsive efficiency was influenced by slip and jet angle, with higher propulsive efficiencies being observed at higher speeds when slip and jet angle were low. Not only are there differences in propulsive efficiency and jet flow features between paralarvae and older life stages but there are also important differences in jet features between juveniles <5.0 cm *DML* and juveniles/adults ≥5.0 cm *DML*. Trends in higher slip, lower propulsive efficiency and high lift production were all noted for squid <5.0 cm *DML*. Moreover, when all the available data were considered, a trend in greater relative use of jet mode I was observed for squid <5.0 cm *DML*. The reasons for these differences are not immediately clear from the results of the present study but they may well be related to ontogenetic difference in the muscular mechanics of the mantle, fins and even the funnel of squids. These areas merit further study.

When the results of the present study are considered collectively with the studies of Anderson and Grosenbaugh (Anderson and Grosenbaugh, 2005), Bartol et al. (Bartol et al., 2008; Bartol et al. 2009), and W.J.S., I.K.B. and P.S.K. (in preparation), it is clear that squids exhibit an impressive locomotive repertoire. Some squids have access to multiple jet modes, including some with $L_{\omega}/D_{\omega}$ near *F*, suggesting that fluid dynamics probably played an integral role in the evolution of squid locomotive systems. It is important to note that despite the ability of squid to form jets with $L_{\omega}/D_{\omega}$s near *F*, they did not always do so. The reasons for this are not yet clear but may be related to the observation that squid in our present study

employed a wide range of fin modes each with distinct kinematic and wake patterns that coordinate with the jet. The consequence of this coordination is that the dual mode propulsive system of squid is complex, involving synergistic interactions between the fin and jet flows: thus a thorough analysis of squid locomotive systems requires simultaneous study of both flows. The dual mode system presents a unique challenge for the identification of hydrodynamic-based gaits in squid, whereby quantitative performance properties (e.g. propulsive efficiency, force production) are ascribed to a defined range of speeds. Only with the aid of powerful new flow quantification tools, such as defocusing DPIV (Pereira and Gharib, 2002; Pereira and Gharib, 2004; Kajitani and Dabiri, 2005; Pereira et al., 2006) that allow for 3-D global quantification of flows in real time around both propulsive systems, will it possible to fully identify hydrodynamic 'gaits' in squid. Although technically challenging, such approaches promise to provide unprecedented data on the dual mode, very unique propulsive system of squids.

## LIST OF ABBREVIATIONS

| | |
|---|---|
| CMP | centrally located mitochondria-rich fibers |
| $D$ | diameter of mechanical jet aperture |
| $D_F$ | diameter of funnel |
| $D_{Fmax}$ | maximum diameter of funnel |
| DML | dorsal mantle length |
| DPIV | digital particle image velocimetry |
| $D_\omega$ | distance between jet vorticity peaks |
| $E$ | kinetic energy of the jet |
| $\bar{E}$ | time-averaged rate at which excess kinetic energy was shed by the jet |
| $F$ | formation number |
| FOV | field of view |
| $\bar{F}_T$ | time-averaged jet thrust |
| $I$ | jet impulse |
| $L$ | distance a piston pushed a column of fluid in a tube |
| $L_V$ | jet length based on the velocity extent |
| $L_\omega$ | jet length based on the vorticity extent |
| $\hat{n}_r$ | unit vector in the radial direction relative to the jet centerline |
| $\hat{n}_z$ | unit vector in the longitudinal direction along the jet centerline |
| $r$ | radial coordinate |
| $Re$ | Reynolds number |
| $Re_{jet}$ | Reynolds number of jet |
| $Re_{squid}$ | Reynolds number of squid |
| SMR | superficially located mitochondria-rich fibers |
| $U$ | mean swimming speed |
| $U_j$ | mean jet velocity along the jet centerline |
| $U_{jmax}$ | peak jet velocity along the jet centerline |
| $U_{jx}$ | horizontal component of mean jet velocity |
| $z$ | longitudinal coordinate along the jet centerline |
| $\eta_p$ | propulsive jet efficiency |
| $\rho$ | fluid density |
| $\psi$ | Stokes stream function |
| $\omega_\theta$ | azimuthal component of vorticity |

## REFERENCES

**Alexander, D. E.** (2002). *Nature's Flyers: Birds, Insects and the Biomechanics of Flight*. Baltimore, MD: Johns Hopkins University Press.

**Alexander, R. M.** (1968). *Animal Mechanics*. Seattle, WA: University of Washington Press.

**Alexander, R. M.** (1977). Storage of elastic strain energy in muscle and other tissues. *Nature* **265**, 114-117.

**Alexander, R. M.** (1986). Human energetics: making headway in Africa. *Nature* **319**, 623-624.

**Alexander, R. M.** (1989). Optimization and gaits in locomotion of vertebrates. *Phys. Rev.* **69**, 1199-1227.

**Alexander, R. M.** (2003). *Principles of Animal Locomotion*. Princeton, NJ: Princeton University Press.

**Anderson, E. J. and DeMont, M. E.** (2005). The locomotory function of the fins in the squid *Loligo pealei*. *Mar. Freshw. Behav. Phys.* **38**, 169-189.

**Anderson, E. J. and Grosenbaugh, M. A.** (2005). Jet flow in steadily swimming adult squid. *J. Exp. Biol.* **208**, 1125-1146.

**Bartol, I. K.** (2001). Role of aerobic and anaerobic circular mantle muscle fibers in swimming squid: electromyography. *Biol. Bull.* **201**, 59-66.

**Bartol, I. K., Mann, R. and Patterson, M. R.** (2001a). Aerobic respiratory costs of swimming in the negatively buoyant brief squid *Lolliguncula brevis*. *J. Exp. Biol.* **204**, 3639-3653.

**Bartol, I. K., Patterson, M. R. and Mann, R.** (2001b). Swimming mechanics and behavior of the negatively buoyant shallow-water brief squid *Lolliguncula brevis*. *J. Exp. Biol.* **204**, 3655-3682.

**Bartol, I. K., Krueger, P. S., Thompson, J. T. and Stewart, W. J.** (2008). Swimming dynamics and propulsive efficiency of squids throughout ontogeny. *Integr. Comp. Biol.* **48**, 720-733.

**Bartol, I. K., Krueger, P. S., Stewart, W. J. and Thompson, J. T.** (2009). Pulsed jet dynamics of squid hatchlings at intermediate Reynolds numbers. *J. Exp. Biol.* **212**, 1506-1518.

**Batty, R. S.** (1984). Development of swimming movements and musculature of larval herring (*Clupea harengus*). *J. Exp. Biol.* **110**, 217-229.

**Biewener, A. A.** (1983). Locomotory stresses in the limb bones of two small mammals: the ground squirrel and chipmunk. *J. Exp. Biol.* **103**, 131-154.

**Biewener, A. A. and Taylor, C. R.** (1986). Bone strain: a determinant of gait and speed? *J. Exp. Biol.* **123**, 383-400.

**Blake, R. W.** (1978). On balistiform locomotion. *J. Mar. Biol. Assoc. UK* **58**, 73-80.

**Boletzky, S. V.** (1987). Embryonic phase. In *Cephalopod Life Cycles*, vol. 2 (ed. P. R. Boyle), pp. 5-31. London: Academic Press.

**Bone, Q., Pulsford, A. and Chubb, A. D.** (1981). Squid mantle muscle. *J. Mar. Biol. Assoc. UK* **61**, 327-342.

**Cavagna, G. A. and Zamboni, A.** (1976). The sources of external work in level walking and running *J. Physiol.* **262**, 639-657.

**Cavagna, G. A., Heglund, N. H. and Taylor, C. R.** (1977). Mechanical work in terrestrial locomotion: two basic mechanisms for minimizing energy expenditure. *Am. J. Physiol.* **233**, 243-261.

**Cheng, J. Y. and DeMont, M. E.** (1996). Jet-propelled swimming in scallops: swimming mechanics and ontogenetic scaling. *Can. J. Zool.* **74**, 1734-1748.

**Childress, S. and Dudley, R.** (2004). Transition from ciliary to flapping mode in a swimming mollusk: flapping flight as a bifurcation in $Re_\omega$. *J. Fluid Mech.* **498**, 257-288.

**Choutapalli, I. M.** (2006). An experimental study of a pulsed jet ejector. PhD Thesis, Florida State University, Tallahassee, FL, USA.

**Costello, J. H., Colin, S. P. and Dabiri, J. O.** (2008). Medusan morphospace: phylogenetic constraints, biomechanical solutions, and ecological consequences. *Invertebr. Biol.* **127**, 265-290.

**Dadswell, M. J. and Weihs, D.** (1990). Size-related hydrodynamic characteristics of the giant scallop, *Placopecten magellanicus* (Bivalvia: Pectinidae). *Can. J. Zool.* **68**, 778-785.

**Daniel, T., Jordan, C. and Grunbaum, D.** (1992). Hydromechanics of swimming. In *Advances in Comparative and Environmetnal Physiology*, vol. 11 (ed. R. M. Alexander), pp. 17-49. London: Springer-Verlag.

**Drucker, E. G. and Jensen, J. S.** (1996). Pectoral fin locomotion in the striped surfperch. II. Scaling swimming kinematics and performance at a gait transition. *J. Exp. Biol.* **199**, 2243-2252.

**Drucker, E. G. and Lauder, G. V.** (1999). Locomotor forces on a swimming fish: three-dimensional vortex wake dynamics quantified using digital particle image velocimetry. *J. Exp. Biol.* **202**, 2393-2412.

**Drucker, E. G. and Lauder, G. V.** (2000). A hydrodynamic analysis of fish swimming speed: wake structure and locomotor force in slow and fast labriform swimmers. *J. Exp. Biol.* **203**, 2379-2393.

**Finke, E. H., Pörtner, O., Lee, P. G. and Webber, D. M.** (1996). Squid (*Lolliguncula brevis*) life in shallow waters: oxygen limitation of metabolism and swimming performance. *J. Exp. Biol.* **199**, 911-921.

**Fuiman, L. A. and Batty, R. S.** (1997). What a drag it is getting cold: partitioning the physical and physiological effects of temperature on fish swimming. *J. Exp. Biol.* **200**, 1745-1755.

**Fuiman, L. A. and Webb, P. W.** (1988). Ontogeny of routine swimming activity and performance in zebra danios (Teleostei: Cyprinidae). *Anim. Behav.* **36**, 250-261.

**Gharib, M., Rambod, E. and Shariff, K.** (1998). A universal time scale for vortex ring formation. *J. Fluid. Mech.* **360**, 121-140.

**Gillis, G. B. and Biewener, A. A.** (2001). Hindlimb muscle function in relation to speed and gait: *in vivo* patterns of strain and activation in a hip and knee extensor of the rat (*Rattus norvegicus*). *J. Exp. Biol.* **204**, 2717-2713.

**Gilly, W. F., Hopkins, B. and Mackie, G. O.** (1991). Development of giant motor axons and neural control of escape responses in squid embryos and hatchlings. *Biol. Bull.* **180**, 209-220.

**Gosline, J. M. and Shadwick, R. E.** (1983). The role of elastic energy storage mechanisms in swimming: an analysis of mantle elasticity in escape jetting in the squid, *Loligo opalescens*. *Can. J. Zool.* **61**, 1421-1431.

**Gosline, J. M., Steeves, J. D., Harman, A. D. and DeMont, E.** (1983). Patterns of circular and radial mantle muscle activity in respiration and jetting of the squid *Loligo opalescens*. *J. Exp. Biol.* **104**, 97-109.

**Hanlon, R. T.** (1990). Maintenance, rearing and culture of teuthoid and sepioid squids. In *Squid as Experimental Animals* (ed. D. L. Gilbert, W. J. Adelman and J. M. Arnold), pp. 35-62. New York: Plenum Press.

**Hanlon, R. T., Hixon, R. F. and Hulet, W. H.** (1983). Survival, growth, and behavior of the loliginid squids *Loligo plei*, *Loligo pealei*, and *Lolliguncula brevis* (Mollusca: Cephalopoda) in closed sea water systems. *Biol. Bull.* **165**, 637-685.

**Hedrick, T. L., Tobalske, B. W. and Biewener, A. A.** (2002). Estimates of circulation and gait change based on a three-dimensional kinematic analysis of flight in cockatiels (*Nymphicus hollandicus*) and ringed turtle-doves (*Streptopelia risoria*). *J. Exp. Biol.* **205**, 1389-1409.

**Hildebrand, M.** (1989). The quadrupedal gaits of vertebrates. *Bioscience* **39**, 766-774.

**Hoar, J. A., Sim, E., Webber, D. M. and O'Dor, R. K.** (1994). The role of fins in the competition between squid and fish. In *Mechanics and Physiology of Animal Swimming* (ed. L. Maddock, Q. Bone and J. M. C. Rayner), pp. 27-33. Cambridge: Cambridge University Press.

**Hove, J. R., O'Bryan, L. M., Gordon, M. S., Webb, P. W. and Weihs, D.** (2001). Boxfishes (Teleostei: Ostraciidae) as a model system for fishes swimming with many fins: kinematics. *J. Exp. Biol.* **204**, 1459-1471.

**Hunter, J. R.** (1972). Swimming and feeding behaviour of larval anchovy *Engraulis mordax*. *Fish. Bull.* **70**, 821-838.

**Jiang, H. and Grosenbaugh, M. A.** (2006). Numerical simulation of vortex ring formation in the presence of background flow: implications for squid propulsion. *Bull. Am. Phys. Soc.* **47**, 96.

**Johnsen, S. and Kier, W. M.** (1993). Intramuscular crossed connective tissue fibres: skeletal support in the lateral fins of squid and cuttlefish. *J. Zool. (Lond.)* **231**, 311-338.

**Kajitani, L. and Dabiri, D.** (2005). A full three-dimensional characterization of defocusing digital particle image velocimetry. *Meas. Sci. Technol.* **16**, 790-804.

**Kier, W. M.** (1989). The fin musculature of cuttlefish and squid (Mollusca, Cephalopoda): morphology and mechanics. *J. Zool. (Lond.)* **217**, 23-38.

**Kier, W. M., Smith, K. K. and Miyan, J. A.** (1989). Electromyography of the fin musculature of the cuttlefish *Sepia officinalis*. *J. Exp. Biol.* **143**, 17-31.

**Korsmeyer, K. E., Steffensen, J. F. and Herskin, J.** (2002). Energetics of median and paired fin swimming, body and caudal fins swimming, and gait transition in parrotfish (*Scarus schlegeli*) and triggerfish (*Rhinecanthus aculeatus*). *J. Exp. Biol.* **205**, 1253-1263.

**Krueger, P. S.** (2001). The significance of vortex ring formation and nozzle exit over-pressure to pulsatile jet propulsion. PhD Thesis, California Institute of Technology, Pasadena, CA, USA.

**Krueger, P. S. and Gharib, M.** (2003). The significance of vortex ring formation to the impulse and thrust of a starting jet. *Phys. Fluids* **15**, 1271-1281.

**Krueger, P. S. and Gharib, M.** (2005). Thrust augmentation and vortex ring evolution in a fully-pulsed jet. *AIAA J.* **43**, 792-801.

**Krueger, P. S., Dabiri, J. O. and Gharib, M.** (2003). Vortex ring pinchoff in the presence of simultaneously initiated uniform background co-flow. *Phys. Fluids* **15**, L49-L52.

**Krueger, P. S., Dabiri, J. O. and Gharib, M.** (2006). The formation number of vortex rings formed in uniform background co-flow. *J. Fluid Mech.* **556**, 147-166.

**Lauder, G. V. and Tytell, E. D.** (2006). Hydrodynamics of undulatory propulsion. In *Fish Biomechanics (vol. 23 Fish Physiology Series)* (ed. R. E. Shadwick and G. V. Lauder), pp. 425-468. Boston, MA: Elsevier Science.

**Lighthill, M. J.** (1960). Note on the swimming of slender fish. *J. Fluid Mech.* **9**, 305-317.

**Lighthill, M. J.** (1975). *Mathematical Biofluidynamics*. Philadelphia, PA: Society for Industrial and Applied Mathematics.

**MacGillivray, P. S., Anderson, E. J., Wright, G. M. and DeMont, M. E.** (1999). Structure and mechanics of the squid mantle. *J. Exp. Biol.* **202**, 683-695.

**McHenry, M. J. and Jed, J.** (2003). The ontogenetic scaling of hydrodynamics and swimming performance in jellyfish (*Aurelia aurita*). *J. Exp. Biol.* **206**, 4125-4137.

**McHenry, M. J. and Lauder, G. V.** (2005). The mechanical scaling of coasting in zebrafish (*Danio rerio*). *J. Exp. Biol.* **208**, 2289-2301.

**McHenry, M. J., Azizi, E. and Strother, J. A.** (2003). The hydrodynamics of locomotion at intermediate Reynolds numbers: undulatory swimming in ascidian larvae (*Botrylloides* sp.). *J. Exp. Biol.* **206**, 327-343.

**McMahon, T. A. and Greene, P. R.** (1979). The influence of track compliance on running. *J. Biomech.* **12**, 893-904.

**Mohseni, K., Ran, H. and Colonius, T.** (2001). Numerical experiments on vortex ring formation. *J. Fluid Mech.* **430**, 267-282.

**Mommsen, T. P., Ballantyne, J., MacDonald, D., Gosline, J. and Hochachka, P. W.** (1981). Analogues of red and white muscle in squid mantle. *Proc. Natl. Acad. Sci. USA* **78**, 3274-3278.

**Müller, U. K., Stamhuis, E. J. and Videler, J. J.** (2000). Hydrodynamics of unsteady fish swimming and the effects of body size: comparing the flow field of fish larvae and adults. *J. Exp. Biol.* **203**, 193-206.

**Nauen, J. C. and Lauder, G. V.** (2002). Hydrodynamics of caudal fin locomotion by chub mackerel, *Scomber japonicus* (Scombridae). *J. Exp. Biol.* **205**, 1709-1724.

**Nauen, J. C. and Shadwick, R. E.** (1999). The scaling of acceleratory aquatic locomotion: body size and tail-flip performance of the California spiny lobster. *J. Exp. Biol.* **202**, 3181-3193.

**Nichols, J. T., Moslemi, A. A. and Krueger, P. S.** (2008). Performance of a self-propelled pulsed-jet vehicle. *AIAA Stud. J.* 2008-3720.

**O'Dor, R. K.** (1988). Forces acting on swimming squid. *J. Exp. Biol.* **137**, 421-442.

**O'Dor, R. K. and Webber, D. M.** (1986). The constraints on cephalopods: why squid aren't fish. *Can. J. Zool.* **64**, 1591-1605.

**O'Dor, R. K., Balch, N., Foy, E. A. and Helm, P. L.** (1986). The locomotion and energetics of hatchling squid, *Illex illecebrosus*. *Am. Malacol. Bull.* **4**, 55-60.

**Otis, T. S. and Gilly, W. F.** (1990). Jet-propelled escape in the squid *Loligo opalescens*: concerted control by giant and non-giant motor axon pathways. *Proc. Natl. Acad. Sci. USA* **87**, 2911-2915.

**Pereira, F. and Gharib, M.** (2002). Defocusing digital particle image velocimetry and the three-dimensional characterization of two-phase flows. *Meas. Sci. Technol.* **13**, 683-694.

**Pereira, F. and Gharib, M.** (2004). A method for three-dimensional particle sizing in two-phase flows. *Meas. Sci. Technol.* **15**, 2029-2038.

**Pereira, F., Stüer, H., Graff, E. C. and Gharib, M.** (2006). Two-frame 3d particle tracking. *Meas. Sci. Technol.* **17**, 1680-1692.

**Preuss, T. Z., Lebaric, N. and Gilly, W. F.** (1997). Post-hatching development of circular mantle muscles in the squid *Loligo opalescens*. *Biol. Bull.* **192**, 375-387.

**Rayner, J. M. V.** (1985). Bounding and undulating flight in birds. *J. Theor. Biol.* **117**, 47-77.

**Robilliard, J. J., Pfau, T. and Wilson, A. M.** (2007). Gait characterization and classification in horses. *J. Exp. Biol.* **210**, 187-197.

**Rome, L. C.** (1994). The mechanical design of the fish muscular system. In *Mechanics and Physiology of Animal Swimming* (ed. L. Maddock, Q. Bone and J. M. V. Rayner), pp. 75-98. Cambridge: Cambridge University Press.

**Rosenfeld, M., Rambod, E. and Gharib, M.** (1998). Circulation and formation number of laminar vortex rings. *J. Fluid Mech.* **376**, 297-318.

**Seibel, B. A., Thuesen, E. V. and Childress, J. J.** (1998). Flight of the vampire: ontogenetic gait-transition in *Vampyroteuthis infernalis* (Cephalopoda: Vampyromorpha). *J. Exp. Biol.* **201**, 2413-2424.

**Spedding, G. R., Rayner, J. M. V. and Pennycuick, C. J.** (1984). Momentum and energy in the wake of a pigeon (*Columbia livia*) in slow flight. *J. Exp. Biol.* **111**, 81-102.

**Spedding, G. R., Rosén, M. and Hedenström, A.** (2003). A family of vortex wakes generated by a thrush nightingale in free flight in a wind tunnel over its entire natural range of flight speeds. *J. Exp. Biol.* **206**, 2313-2344.

**Thompson, J. T. and Kier, W. M.** (2001). Ontogenetic changes in mantle kinematics during escape-jet locomotion in the oval squid, *Sepioteuthis lessoniana* Lesson, 1830. *Biol. Bull.* **201**, 154-166.

**Thompson, J. T. and Kier, W. M.** (2002). Ontogeny of squid mantle function: changes in the mechanics of escape-jet locomotion in the oval squid, *Sepioteuthis lessoniana* Lesson, 1830. *Biol. Bull.* **203**, 14-26.

**Thompson, J. T. and Kier, W. M.** (2006). Ontogeny of mantle musculature and implications for jet locomotion in oval squid *Sepioteuthis lessoniana*. *J. Exp. Biol.* **209**, 433-443.

**Thompson, J. T., Szczepanski, J. A. and Brody, J.** (2008). Mechanical specialization of the obliquely striated circular mantle muscle fibres of the long-finned squid *Doryteuthis pealeii*. *J. Exp. Biol.* **211**, 1463-1474.

**Vecchione, M., Young, R. E., Guerra, A., Lindsay, D. J., Clague, D. A., Bernhard, J. M., Sager, W. W., Gonzalez, A. F., Rocha, F. J. and Segonzac, M.** (2001). Worldwide observations of remarkable deep-sea squids. *Science* **294**, 2505-2506.

**Vecchione, M., Roper, C. F. E., Widder, E. A. and Frank, T. M.** (2002). *In situ* observations on three species of large-finned deep-sea squids. *Bull. Mar. Sci.* **71**, 893-901.

**Vecchione, M., Shea, E., Bussarawit, S., Anderson, F., Alexeyev, D., Lu, C. C., Okutani, T., Roeleveld, M., Chotiyaputta, C., Roper, C. et al.** (2005). Systematic of Indo-West Pacific loliginids. *Phuket Mar. Biol. Cent. Res. Bull.* **66**, 23-26.

**Videler, J. J.** (1993). *Fish Swimming*. London: Chapman & Hall.

**Vogel, S.** (2003). *Comparative Biomechanics: Life's Physical World*. Princeton, NJ: Princeton University Press.

**Webb, P. W.** (1971). The swimming energetics of trout. I. Thrust and power output at cruising speeds. *J. Exp. Biol.* **55**, 489-520.

**Webb, P. W.** (1993). Is tilting at low swimming speeds unique to negatively buoyant fish? Observations on steelhead trout, *Oncorhynchus mykiss*, and bluegill, *Lepomis macrochirus*. *J. Fish. Biol.* **43**, 687-694.

**Webb, P. W.** (1994). The biology of fish swimming. In *Mechanics and Physiology of Animal Swimming* (ed. L. Maddock, Q. Bone and J. M. V. Rayner), pp. 45-62. Cambridge: Cambridge University Press.

**Webb, P. W.** (1998). Entrainment by river chub, *Nocomis micropogon*, and smallmouth bass, *Micropterus dolmieu*, on cylinders. *J. Exp. Biol.* **201**, 2403-2412.

**Webb, P. W.** (2006). Stability and maneuverability. In *Fish Biomechanics* (ed. R. E. Shadwick and G. V. Lauder), pp. 281-332, Elsevier: New York.

**Webb, P. W. and Gerstner, C. L.** (2000). Swimming behaviour: predictions from biomechanical principles. In *Biomechanics in Animal Behaviour* (ed. P. Domenici and R. W. Blake), pp. 59-77. Oxford: Bios Scientific.

**Webb, P. W. and Weihs, D.** (1986). Functional locomotor morphology of early life history stages of fishes. *Trans. Am. Fish. Soc.* **115**, 115-127.

**Westerweel, J., Dabiri, D. and Gharib, M.** (1997). The effect of a discrete window offset on the accuracy of cross-correlation analysis of digital PIV recordings. *Exp. Fluids* **23**, 20.

**Wilga, C. D. and Lauder, G. V.** (2004). Hydrodynamic function of the shark's tail. *Nature* **430**, 850.

**Willert, C. E. and Gharib, M.** (1991). Digital particle image velocimetry. *Exp. Fluids* **10**, 181-193.

**Williams, T. A.** (1994). A model of rowing propulsion and the ontogeny of locomotion in *Artemia* larvae. *Biol. Bull.* **187**, 156-163.

**Wu, T. Y.** (1977). Introduction to the Scaling of Aquatic Locomotion. In *Scale Effects in Animal Locomotion* (ed. T. J. Peldley), pp. 203-232. London: Academic Press.